An Analysis of the Stability Characteristics of Celo

cLabs Team*

DRAFT version 0.16

Abstract

Celo is a decentralized platform that will enable a family of crypto-collateralized/seigniorage-style stable value assets. This document analyzes the behavior of Celo stable value assets over a set of simulated scenarios.

*cLabs is one of the teams working on Celo.

Contents

1 Introduction

The Celo protocol [5] defines a decentralized payments system in which participants use coins that track the value of a local fiat currency or a local basket of goods. In this paper, we investigate the stability characteristics of Celo stable value assets through a series of simulations under various market conditions. For simplicity, we focus on the case of a single asset, called the Celo Dollar, that tracks the value of the US Dollar.

1.1 Stability Mechanism

The Celo protocol, at base, has two assets: Celo Dollar, an elastic-supply stable value asset[1], and CELO[2], a fixed-supply variable value asset. CELO is the utility token of the protocol and serves multiple purposes. It is, for example, a central component of the consensus and governance mechanism of the Celo protocol as voting power in validator elections and governance decisions is proportional to the amount of CELO locked for voting. CELO is also elementary to the stability mechanism: It is held in a reserve smart-contract and exchanged for Celo Dollars to balance demand excess or shortage. In addition to CELO, a diversified basket of non-Celo crypto-assets comprises the Celo reserve. This reserve is periodically rebalanced towards target asset allocation set via on-chain governance. The Celo stability mechanism can thus be understood as hybrid crypto-collateralization / seigniorage-style model.

To balance Celo Dollar demand excess or shortage, the protocol sets incentives for users to adjust Celo Dollar supply to match Celo Dollar demand at the price target. At a high level, the Celo expansion and contraction mechanism allows users to create new Celo Dollars by sending one US Dollar worth of CELO to the reserve, or to burn Celo Dollars by redeeming them for one US Dollar worth of CELO. This mechanism, referred to as decentralized one-to-one mechanism (DOTO) for the rest of this article, creates incentives such that when demand for the Celo Dollar rises and the market price is above the target, an arbitrage profit can be achieved by buying one US Dollar worth of CELO on the market, exchanging it with the protocol for one Celo Dollar, and selling that Celo Dollar for the market price. Similarly, when demand for the Celo Dollar falls and the market price is below the target, an arbitrage profit can be achieved by purchasing Celo Dollars at the market price, exchanging it with the protocol for one US Dollar worth of CELO, and selling the CELO to the market. These actions are expected to drive the market price of the Celo Dollar back towards one US Dollar without the need for the protocol to estimate the optimal expansion or contraction amounts. The exact expansion and contraction mechanism, which includes some additional features, is described and analyzed in more detail in Section 4.3.1.

1.2 Stability Risks

The primary risk to Celo Dollar stability is a scenario in which there is a decrease in demand for Celo Dollars greater than the total value of the reserves. In such a scenario, the protocol would be unable to handle a sufficient contraction amount to meet decreased demand.

A secondary risk is a scenario in which there exists enough value in the reserves to handle a contraction in demand, but not enough market liquidity to sell the amount of crypto assets quickly enough to handle the contraction.[3]

To obtain an estimate of the likelihood of either of these risks under the given modelling assumptions, we would need to model the demand for Celo Dollars, the value of the reserves, the flows of Celo currency through the expansion and contraction mechanism and other major stability related mechanics of the Celo protocol. We do so in the next four sections.

2 Scenario Generation

In this section we describe the scenario generator that creates the scenarios for the analysis of the stability mechanism. Paragraph 2.1 provides a non-technical introduction and motivation of the

[1] In actuality, the Celo protocol allows for many stable value assets and many reserve assets [5]. However, the analysis of the base case is generalizable to the multiple-asset case.

[2] CELO, the Celo native asset, was previously called Celo Gold or cGLD, and the name changed to CELO after a community-driven governance proposal in June 2020.

[3] A similar risk occurs if the protocol cannot buy crypto assets quickly enough to handle an expansion in demand.

scenario generation framework used in this paper. Technical details regarding the model choice are covered in Appendix A. Section 2.2 provides a short description of the stochastic process that we consider for the scenario generator. The final parameter settings used for the simulation of Celo Dollar demand and the value of crypto assets for the analysis in this article are discussed in Section 3 and 4.2.3, respectively.

2.1 Non-Technical Introduction

At the core of our analysis is a Monte Carlo simulation that generates values for the key factors that affect stability – principally, Celo Dollar demand, and the prices of the crypto assets in the reserve. It is our intention to create a wide range of plausible scenarios that include steep downturns as well as upturns, and to take into account scenarios that expose the stability mechanism to the risks outlined in Section 1.2.

We do not seek to forecast the future evolution of markets or to perform distribution fitting to historical market data. Our simulation analysis covers up to 30 years, and long-term forecasts cannot provide reliable results for such time scales. There exist attempts to analyse the distribution of cryptocurrency prices (see f.ex. [2] or [10]), that all come to similar conclusions with regard to general statistical shapes and characteristics. As expected, the results indicate that cryptocurrency prices have semi-heavy or heavy tailed distributions. Yet there is disagreement with regard to the distributions that provide the best statistical fit to the prices of individual cryptocurrencies. Apart from methodological differences in the analyses, the differences might partially be caused by different time intervals of historical data that have been chosen. It clearly indicates that successfully fitting a distribution requires a challenging analysis on its own, and that, to no surprise, results are highly dependent on time periods.

Our current setup provides scenario generators that create paths from geometric Brownian motions and geometric Ornstein-Uhlenbeck processes. The geometric Brownian motion is a widely used stochastic process. It has been used in the analysis of other stable coin projects [1], [9] and also in earlier versions of this stability analysis. However, depending on the parameter settings, the geometric Brownian motion produces scenarios that tend to be unbalanced or even decaying to 0 evolving in time. In Figure 1 we have provided examples of three regimes of scenarios that can occur. Each graph shows the evolution of 100 paths of a geometric Brownian motion simulated with the same volatility parameter $\sigma = 0.75$ and different drift parameters (drift $\mu = 0$, $\frac{1}{2}\sigma^2$ and 0.5). The characteristic behaviour of the evolution of the paths is visible: decay to 0, fluctuation around the initial value and divergence to ∞. For example, Figure 1a shows significant downward evolution of a large proportion of paths. The thick, colourful lines indicate the proportion of paths that are below the line; 75% of the paths are below the red line and decay below a level of at least approximately 0.0035 after 30 years. In other words a very large proportion of scenarios represent downturn scenarios, and with time the number of downturn scenarios is increasing until eventually almost all paths will be downturn scenarios. A more technical description and explanation of this behaviour is provided in Appendix A.

In contrast to the geometric Brownian motion, the geometric Ornstein-Uhlenbeck process has a stationary distribution and converges towards it in time. As a consequence, scenarios of a geometric Ornstein-Uhlenbeck process will not decay to 0 or diverge to ∞. In Figure 2 we have provided examples of scenarios for parameter settings corresponding to the three examples in Figure 1. Over time the proportions of paths within a fixed range settles as the process converges to its stationary distribution. For example, Figure 2a shows large proportions of paths having a downwards trend initially. As before, the thick, colourful lines indicate the proportion of paths below the line. Towards year 30 the slope of these lines decreases increasingly and eventually would converge to 0. Therefore, the percentiles will not decay to 0.

In order to acknowledge the heavy tails that are observed in price distributions of cryptocurrencies, we equip both processes with an additional jump process. The occurrence of a jump is determined by a Poisson process and jump sizes are log-normally distributed random variables, a setup referred to as compound Poisson process with log-normal jump sizes. On path-level, jumps introduce movements that are more extreme than those of the geometric Brownian motion or the geometric Ornstein-Uhlenbeck process.

Celo Dollar demand and multiple crypto assests are simulated as a multivariate process, i.e. they are simulated simultaneously and feature correlation between the different crypto assets as well as correlation between Celo Dollar demand and crypto assets.

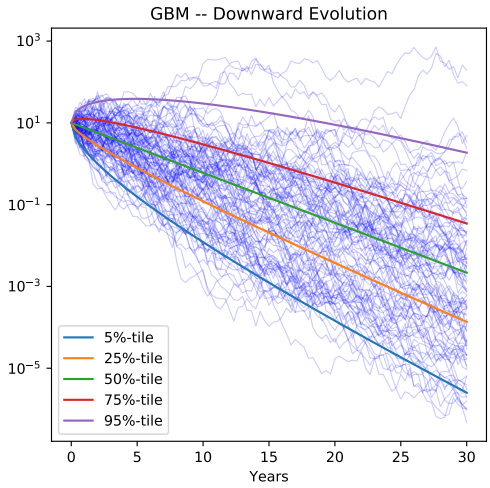

(a) Percentiles and paths of the geometric Brownian motion with drift $\mu = 0$ and volatility $\sigma = 0.75$. Eventually, all percentiles are decreasing and converging to 0. Due to the logarithmically scaled y-axis convergence or divergence speeds might seem to be much lower than they really are; exponential behaviour appears to be only linear.

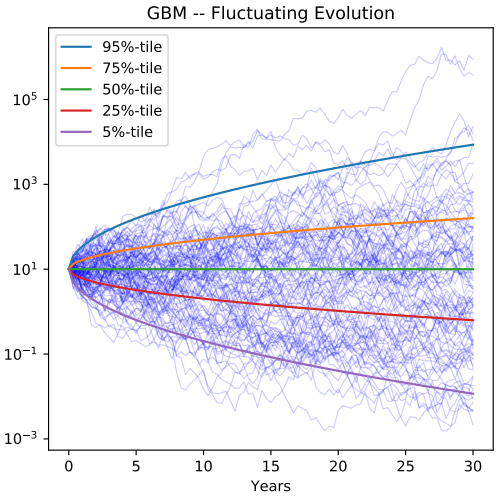

(b) Percentiles and paths of the geometric Brownian motion with drift $\mu = \frac{1}{2}\sigma^2$ and volatility $\sigma = 0.75$. At each time 50% of the mass is above and 50% is below the initial value. This specific choice of μ is the only the parameter setting for which paths and percentiles are not decaying to 0 or diverging to ∞. Due to the logarithmically scaled y-axis convergence or divergence speeds might seem to be much lower than they really are; exponential behaviour appears to be only linear.

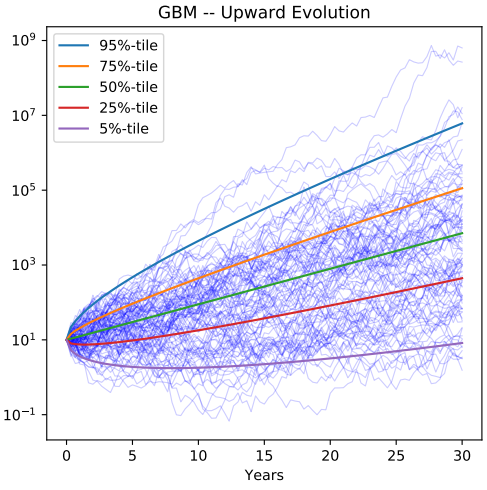

(c) Percentiles and paths of the geometric Brownian motion with drift $\mu = 0.5$ and volatility $\sigma = 0.75$. Eventually, all percentiles are increasing and diverging to ∞. Due to the logarithmically scaled y-axis convergence or divergence speeds might seem to be much lower than they really are; exponential behaviour appears to be only linear.

Figure 1

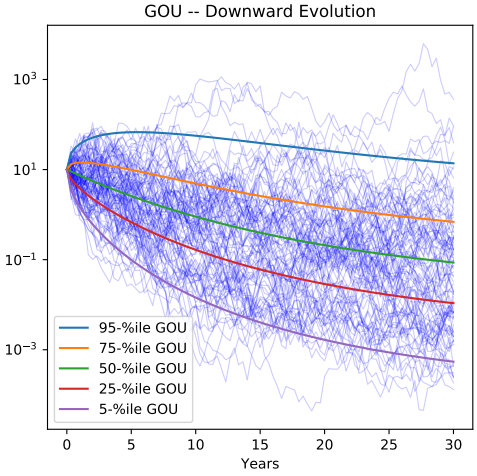

(a) Percentiles and paths of the geometric Ornstein-Uhlenbeck process with mean reversion speed $\kappa = 0.05$, volatility $\sigma = 0.75$ and drift parameter $\Theta = 7.06$. The parameters are calibrated such that the expectation value at time $t = 30$ years is equal to the initial value. Eventually, the slope of all percentiles will decrease to 0 and all percentiles will be constant. The paths will not decay to 0. Due to the logarithmically scaled y-axis convergence or divergence speeds might seem to be much lower than they really are; exponential behaviour appears to be only linear.

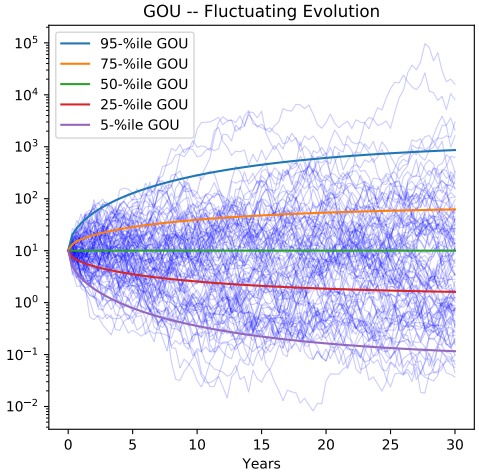

(b) Percentiles and paths of thegeometric Ornstein-Uhlenbeck process with mean reversion speed $\kappa = 0.03$, volatility $\sigma = 0.75$ and drift parameter $\Theta = 11.68$. At each time 50% of the mass is above and 50% is below the initial value. Due to the logarithmically scaled y-axis convergence or divergence speeds might seem to be much lower than they really are; exponential behaviour appears to be only linear.

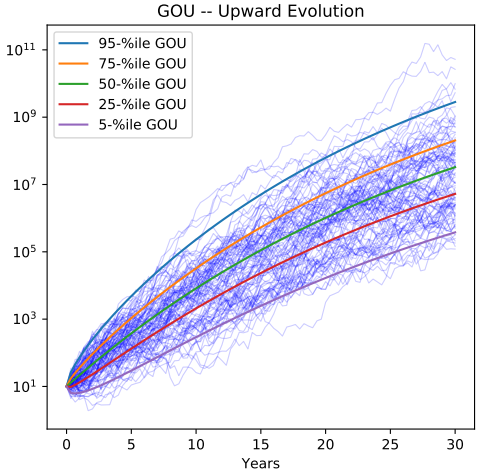

(c) Percentiles and paths of the geometric Ornstein-Uhlenbeck process with mean reversion speed $\kappa = 0.03$ and drift parameter $\Theta = 36.95$. The parameters are calibrated such that the expectation value at time $t = 30$ years is equal to $10e^{0.5\times30}$, the expectation value of the GBM in Figure 1c. Eventually, the slope of all percentiles will decrease to 0 and all percentiles will be constant. The paths will not diverge to ∞. Due to the logarithmically scaled y-axis convergence or divergence speeds might seem to be much lower than they really are; exponential behaviour appears to be only linear.

Figure 2

2.2 Stochastic Processes

As discussed above the stochastic process used for the simulation of Celo Dollar demand and the value of the crypto assets can be either a multivariate geometric Brownian motion or a multivariate geometric Ornstein-Uhlenbeck with jumps from a compound Poisson process with log-normal jump sizes. In this section we provide a short description of the multivariate process without including many details about the specific application to the case of Celo Dollar demand or crypto assets. These details including the individual parameter settings are discussed in Sections 3.1 and 4.2.3.

Geometric Brownian Motion: In the case of the geometric Brownian motion the process X_t^i, $i = 1, \ldots, n$ is defined by the following equation

$$X_t^i = X_0^i \exp\left((\mu_i - \frac{1}{2}(\sigma^i)^2)t + \sigma_i W_t^i\right) \prod_{j=1}^{N_t^i} \exp(Y_j^{i,idio}) \prod_{j=1}^{N_t} \exp(Y_j^{syst}) \ , \tag{1}$$

where μ_i is the drift parameter, σ_i is the volatility parameter of process X_t^i and $\{W_t^i\}$, $i = 1, \ldots, n$ are Brownian motions with correlation ρ^{ij}. Each process X_t^i has an idiosyncratic jump component with Poisson process N_t^i with intensity λ_{idio}^i and jump size $Y_t^{i,idio}$. The jump size random variables $Y_t^{i,idio}$ are independent from one another and the Poisson process and identically distributed with a normal distribution with parameters μ_{idio}^i and σ_{idio}^i

$$Y_t^{i,idio} \sim \mathcal{N}\left(\mu_{idio}^i, (\sigma_{idio}^i)^2\right) \ . \tag{2}$$

Crypto assets have an additional systematic jump component with Poisson process N_t with intensity λ_{syst} and jump size Y_i^{syst}. The systematic jump size Y_i^{syst} is independent from the Poisson process and identically distributed with normal distribution with parameters μ_{syst} and σ_{syst}

$$Y_t^{syst} \sim \mathcal{N}\left(\mu_{syst}, \sigma_{syst}^2\right) \ . \tag{3}$$

Geometric Ornstein-Uhlenbeck: In the case of the geometric Ornstein-Uhlenbeck the process X_t^i, $i = 1, \ldots, n$ is given by

$$\begin{aligned} X_t^i = \left(X_0^i\right)^{e^{-\kappa t}} \exp\left((\theta_i - \frac{\sigma_i^2}{2\kappa_i})(1 - e^{-\kappa t}) + \int_0^t \sigma_i e^{-\kappa(t-s)}\, dW_s^i\right) \\ \times \prod_{j=1}^{N_t^i} \exp(Y_j^{i,idio})^{e^{-\kappa_i(t-t_j)}} \prod_{j=1}^{N_t} \exp(Y_j^{syst})^{e^{-\kappa_i(t-t_j)}} \ , \end{aligned} \tag{4}$$

where κ_i is the mean reversion speed parameter, Θ_i the drift parameter σ_i is the volatility parameter of process X_t^i and $\{W_t^i\}$, $i = 1, \ldots, n$ are Brownian motions with correlation ρ^{ij}. Each process X_t^i has an idiosyncratic jump component with Poisson process N_t^i with intensity λ_{idio}^i and jump size $Y_t^{i,idio}$. The jump size random variables $Y_t^{i,idio}$ are independent from one another and the Poisson process and identically distributed with a normal distribution with parameters μ_{idio}^i and σ_{idio}^j

$$Y_t^{i,idio} \sim \mathcal{N}\left(\mu_{idio}^i, (\sigma_{idio}^i)^2\right) \ . \tag{5}$$

Crypto assets have an additional systematic jump component with Poisson process N_t with intensity λ_{syst} and jump size Y_i^{syst}. The systematic jump size Y_i^{syst} is independent from the Poisson process and identically distributed with normal distribution with parameters μ_{syst} and σ_{syst}

$$Y_t^{syst} \sim \mathcal{N}\left(\mu_{syst}, \sigma_{syst}^2\right) \ . \tag{6}$$

3 Demand: A Stochastic Anchor Point Model

The demand quantity Q_t represents the demand for Celo Dollars at the price of one US Dollar and is simulated as one of the processes of the multivariate stochastic process used for the scenario generator. In Section 3.1 we provide details about the specific setup and the parameter setting of the demand process used for the stability analysis. Changes of demand lead to an demand excess or shortage and may trigger the expansion and contraction mechanism (see Section 4.3).

Parameter	Value
Q_0	20 000 000
κ_d	0.001
Θ_d	$\ln Q_0 + \frac{\sigma^2}{2\kappa}$
σ_d	1
λ^d_{idio}	5
μ^d_{idio}	0
σ^d_{idio}	0.3

Table 1: Parameter setting used for the simulation of the Celo Dollar demand quantity Q_t for the analysis of the stability mechanism (see Section 5).

3.1 Model Choice and Parameter Setting

With the parameter setting of the Celo Dollar demand process we are trying to take into account the requirements for the scenario generation that we have outlined in Section 2. It is our intention to create a wide range of plausible scenarios that include steep downturns as well as upturns and to take into account scenarios that expose the stability mechanism to the stability risks outlined in Section 1.2.

Model Choice: We choose a geometric Ornstein-Uhlenbeck process with jumps from a compound Poisson process for the scenario generation (see Section 2.2). The reasons are explained in a non-technical way in Section 2 (see Appendix A for a more technically involved discussion).

Parameter Setting: We choose a drift parameter Θ_d such that 50% of the paths are above and 50% are below the initial value. By rearranging Equation (68) and using $p_{\mathcal{N}}(50\%) = 0$, the drift parameter Θ_d can be expressed as a function of κ_d, σ_d and the target value at time t

$$\Theta_d = \frac{1}{1 - e^{-\kappa_d t}} \left(\ln \text{ target} - e^{-\kappa_d t} \ln Q_0 \right) + \frac{\sigma_d^2}{2\kappa_d} \ . \tag{7}$$

Our target value is the assumed initial demand Q_0. Therefore the drift parameter Θ_D is given by

$$\Theta_d = \ln Q_0 + \frac{\sigma_d^2}{2\kappa_d} \ . \tag{8}$$

Crypto markets exhibit a comparably high volatility; annualised volatilities[4] around 1 or significantly above 1 are common. These volatilities can be observed for prices as well as market capitalisation. While it is indeed arguable, whether the volatility of price returns is a good indicator for the volatility of demand, the market capitalisation of a stable coin might be considered as a proxy value for the demand at the price target. We use the magnitude of the observed volatilities to have a rough estimate. As the percentiles of the process scale with the parameter σ_d, i. e. larger σ_d values create wider percentiles (see Equation (68)), the final parameter is ultimately set such that it yields sufficiently wide percentiles. With the final parameter setting (see Table 1) the ranges limited by the 5th and 95th and the 1st and 99th percentile at $t = 30$ years are approximately $[4 \times 10^4, 5 \times 10^{13}]$ and $[6 \times 10^2, 3 \times 10^{15}]$. Figure 3 shows the evolution of a few percentiles obtained with the same parameter setting.

The mean reversion parameter κ_d has influence on how fast the percentiles become constant which prevents the decay and divergence that can occur with geometric Brownian motions (see Section 2). In the case of the specific parameter setting of the drift parameter θ_d (constant 50th percentile) we do not really require this feature of the geometric Ornstein-Uhlenbeck process. Hence, we set the mean reversion speed to a low value $\kappa_d = 0.001$.

For the jump process we follow the idea of the heuristic 3σ rule according to which events that deviate more than three standard deviations from the mean are considered to be an outlier. With a volatility parameter of $\sigma_d = 1$, we set the standard deviation of the jump size process $\sigma^d_{idio} = 0.3$. We have obtained this value by rounding down $6\frac{\sigma_d}{\sqrt{360}} = \frac{6}{\sqrt{360}}$, i.e. six times the daily volatility

[4]Standard deviation of log-returns

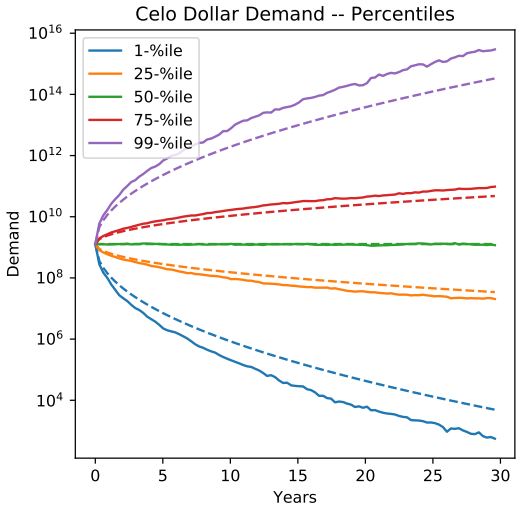

Figure 3: This figure shows empirical percentiles (sample size = 10 000) of the Celo Dollar demand processes using the parameter settings summarised in Table 1. As a reference the dashed lines show the theoretical percentiles of a geometric Ornstein-Uhlenbeck process without jumps. At each time t, 50% of the paths are above the initial value and 50% of the paths are below the initial value.

$\frac{\sigma_d}{\sqrt{360}}$. In case of a normal distribution an event of larger or equal to 3σ occurs with probability 0.3%, which would be approximately once in 360 days. We set the jump intensity of the Poisson process $\lambda^d_{idio} = 5$ to have five additional events per year on average. The jump process leads to an additional widening of the percentiles. This can been seen in Figure 3 by comparing the solid lines with the dashed lines.

3.2 Shape of the Demand Curve

For each stochastic anchor point simulated via the stochastic model described in the last section, we span a demand curve assuming the following functional form

$$q_t = \frac{Q_t}{p_t} \tag{9}$$

where the stochastic anchor point Q_t gives the demand at the \$1 price target generated by the stochastic model, and q_t denotes the demand at price p_t. [5] This demand curve model allows to calculate the price of Celo Dollars in cases where supply cannot match demand – see, for example, Figure 4, a scenario in which the demand for Celo Dollars (at 1 US Dollar) at time step t is $Q_t = 20M$. If Celo Dollar supply is $20M$ coins (green line), then the peg is maintained in this simulation. If Celo Dollar supply is only $19M$ (for example due to constrained liquidity, orange line), a Celo Dollar price of \$1.05 results.

3.3 Modeling Demand Downward Pressure

Celo Dollar demand might not be entirely exogenous but could be affected by the value of the Celo reserve. In other words, low reserve ratios may lead to lower demand for Celo Dollars. The Celo reserve and how it is modeled in this analysis is discussed in detail in Section 4.2.

To account for potential downwards pressure on Celo Dollar demand in times in which the Celo reserve is low, we model a demand multiplier M^d_t that reduces the simulated Celo Dollar demand in response to a low reserve. More precisely, the pre-generated Celo Dollar demand anchor points Q_t are multiplied by M^d_t which is modeled as the following piece-wise linear function of the crypto-reserve-ratio rr^c_t

[5] This is an initial modeling assumption; in future work we will explore how sensitive our stability results are with respect to changes in the elasticity of demand.

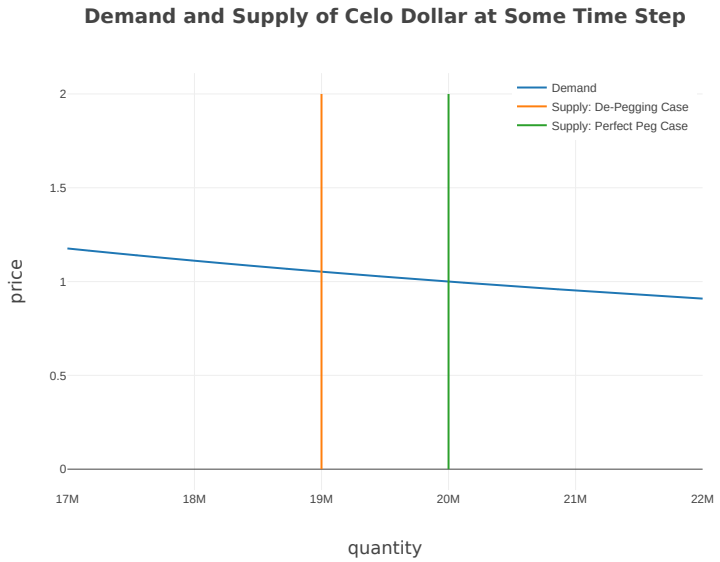

Figure 4: This Figure shows an example demand curve for Celo Dollars in our model. In this, case a demand for $Q_t = 20\text{M}$ coins is generated via a stochastic process. The rest of the demand curve is then constructed around this anchor by assuming the parametric form of the demand curve described by Equation (9). This setup allows us to model the price of Celo Dollars in cases where the protocol is unable to expand or contract the supply sufficiently.

$$M_t^d = \begin{cases} 1 & \text{if } rr_t^c \geq \tau^d \\ \frac{rr_t^c}{\tau^d} & \text{if } 0 \leq rr_t^c < \tau^d \end{cases}, \tag{10}$$

where rr_t^c is defined as the ratio of the US Dollar value of the non-Celo part of the reserve over the total Celo Dollar supply. The simulations conducted in this analysis assume $\tau^d = 0.5$. This implies that the Celo Dollar demand at the target is discounted as soon as the value of the non-Celo part of the Celo reserve drops below a level at which it could cover 50% of the total Celo Dollar supply.

The above demand multiplier can lead to demand downward spirals as a drop in Celo Dollar demand leads to a contraction of supply, which in times of a already low crypto-reserve-ratio decreases the multiplier, which in turn reduces the Celo Dollar demand further, and so forth. The downward spiral effect is especially pronounced when a similar multiplier is introduced for the value of CELO. Such a multiplier is also used in this analysis and discussed in Section 4.2.4.3.

3.4 Market Correlation

As described in Section 2.2 Celo Dollar demand and crypto asset prices are generated by a multivariate process. We set the correlation between demand and crypto asset prices to a positive value to take into account scenarios in which a global dynamic of the crypto market affects demand and crypto asset prices. In particular, a simultaneous decrease in demand and crypto asset prices is a risk driver for the stability of the mechanism (see Section 1.2).

The correlations ρ_{d,a_i} between the Celo Dollar demand and the crypto assets are generated by truncated normal random variables restricted to $[-1, 1]$ with probability density function

$$f(x, \mu_\rho, \sigma_\rho) = \frac{\phi\left(\frac{x-\mu_\rho}{\sigma_\rho}\right)}{\Phi\left(\frac{1-\mu_\rho}{\sigma_\rho}\right) - \Phi\left(\frac{-1-\mu_\rho}{\sigma_\rho}\right)}, \tag{11}$$

where μ_ρ is the mean parameter, σ_ρ the volatility parameter and ϕ and Φ are the probability density and the distribution function of the standard normal distribution, respectively. For the simulation analysis we set the mean parameter $\mu_\rho = 0.5$ and the volatility parameter $\sigma_\rho = 0.05$. As a consequence the correlations ρ_{d,a_i} between Celo Dollar demand and the crypto asset will be around 0.5.

4 Supply: Matching the Demand to Stabilize the Price

The last section describes the stochastic model used to generate Celo Dollar demand scenarios in this simulation analysis. This section explains how protocol driven supply adjustments in response to demand changes are modeled. Section 4.1 outlines how supply adjustments are achieved by assuming a representative agent that takes all arbitrage opportunities when interacting with the Celo expansion and contraction mechanism. Sections 4.2 and 4.3 explain the constraints to adjusting supply, namely the value of the Celo reserve and the liquidity constraints introduced via the Celo expansion and contraction mechanism.

4.1 Adjusting Supply

This section explains on a high level how supply adjustments are calculated in this simulation analysis. With CP-DOTO participants have the constant possibility to interact with the expansion and contraction mechanism. For the sake of this simulation analysis, we have modelled a step-wise approach: We assume that at $t = 0$, the market is in an equilibrium state and the demand Q_0 is matching the supply $S_0 = Q_0$ resulting in a Celo Dollar price of one. At time $t = 1$ the demand has been changed to Q_1 by the scenario generator. Unless $Q_1 = S_0$, the demand excess or shortage $Q_1 - S_0$ causes the Celo Dollar price to deviate from 1. In case of a depeg the expansion and contraction mechanism (see Section 4.3) is triggered and adjusts the supply from S_0 to S_1. Based on the demand Q_1 and the supply S_1 the price p_1 is calculated. In the next step the demand changes to Q_2 leading to a potential demand excess or shortage of $Q_2 - S_1$ which again triggers the expansion and contraction mechanism. More generally, at time t we are starting with a demand quantity Q_t and a supply S_t. The scenario generator creates a new demand quantity Q_{t+1}. If the new demand leads to a demand excess or shortage $Q_{t+1} - S_t$ causing the Celo Dollar price to deviate, the expansion and contraction mechanism is triggered and adjusts the supply from S_t to S_{t+1}. As a result, at time $t + 1$ we have a demand quantity Q_{t+1}, a supply of S_{t+1} and a Celo Dollar price p_{t+1}. These steps are illustrated in Figure 5.

There are two main constraints to adjusting Celo Dollar supply: the value of the reserve (the supply of Celo Dollars cannot contract by more than the value of the reserve), and liquidity (the supply of Celo Dollars cannot expand or contract quicker than the market's willingness to sell or buy reserve assets through the expansion and contraction mechanism).

Section 4.2 describes how the reserve value is modeled whereas Section 4.3 explains how market liquidity and the Celo expansion and contraction mechanism is modeled.

4.2 Constraints to Adjusting Supply: The Value of the Reserve

The protocol cannot contract more Celo Dollar supply than the value of the reserve. This section describes how the value of the reserve is modeled in our simulation analysis.

4.2.1 Bootstrapping the Reserve

The reserve portfolio is bootstrapped from CELO that is initially allocated to the reserve. A fraction of this CELO is exchanged to a basket of non-Celo crypto assets that is also deposited in the reserve to reach an initial reserve target allocation.

With both, CELO and non-Celo assets in the reserve, Celo Dollars can be purchased into existence via the stability mechanism and are additionally backed by the new reserve assets used for the purchase. Our analysis assumes that the initial reserve shows a balance of $G^{reserve} = 120$ million CELO coins and that the total number is limited to $G^{total} = 1$ billion, which is the maximum number of CELO coins ever to exist in the actual production network.

4.2.2 Reserve Asset Allocation

The reserve consists of CELO and a diversified basket of non-Celo crypto assets, and is periodically rebalanced to achieve a target ratio r^g of CELO and non-Celo assets[6].

For modeling purposes, we assume an equal weighting of $N = 3$ volatile crypto assets for the non-Celo portion of the reserve, with bi-weekly rebalancing for this simulation ($f_{bal} = 14$). We

[6]The target ratio in our model is 1:1, so that 50% of the reserve is held as CELO, and 50% is held as a diversified basket of cryptocurrencies.

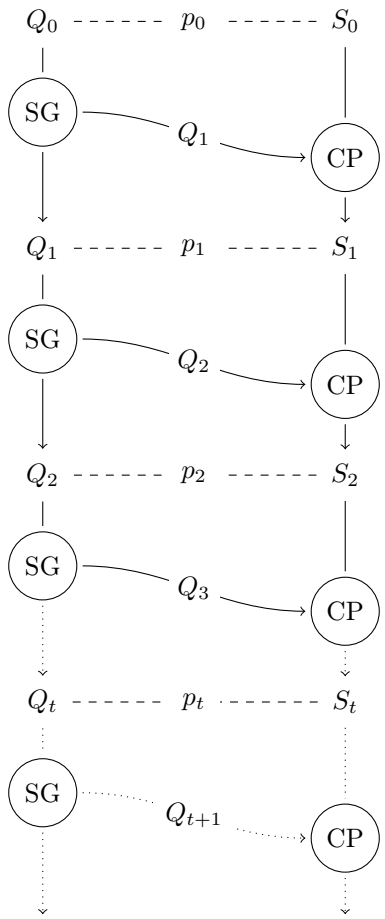

Figure 5: Flow chart of the Celo Dollar demand and supply progression in the simulation. p_t denotes the price that results from the demand and supply quantity given at time t. SG represents the scenario generator that provides the next demand quantity. Whenever the Celo Dollar price deviates from 1, the expansion and contraction mechanism is triggered and adjusts the supply. The expansion and contraction mechanism, called CP-DOTO, is denoted CP. The position of the CP node is deliberately displaced with respect to the SG node as the contraction and expansion mechanism responds to changes of the demand by the scenario generator.

chose this approach – as opposed to more passive methods like market-cap weighted indexing, or more active methods like those described by Markowitz ([7], optimize risk/return), Kelly ([6], optimize log-utility), or Michaud ([8], include estimation risk in defining portfolio optimality) – because market-cap weighted indexing would lead to high single-asset concentrations and methods like Kelly, Markowitz or Michaud are highly dependent on input parameters. In finance literature, portfolios based on a naive 1/N heuristic are standard benchmarks to more sophisticated allocation methods, and in our case, a portfolio constructed in this manner would provide a comprehensible lower-bound for this stability analysis.

In addition to the N volatile assets, we assume that there are non-volatile reserve crypto assets with a initial annual default probability of $\lambda_{default}$ and that this default probability declines linearly to 0 over the simulated 30 year period. Reserve rebalancings are conducted such that a fraction h of the non-Celo reserve is held in this non-volatile asset after rebalancing is completed. The fraction h is modeled as a linear function of the crypto-reserve-ratio rr_t^c, i.e. the Celo Dollar supply over the US Dollar value of the non-Celo crypto reserve. More precisely,

$$h_t = \begin{cases} 1 & \text{if } rr_t^c < \tau_1^r \\ 1 - \frac{rr_t^c - \tau_1^r}{\tau_0^r - \tau_1^r} & \text{if } rr_t^c \in [\tau_1^r, \tau_0^r] \\ 0 & \text{if } rr_t^c > \tau_0^r \end{cases} \tag{12}$$

In this analysis, we assume $\tau_1^r = 0.75$ and $\tau_0^r = 1.5$

Parameter	Value
A_0	normalised to 1
κ_a	0.001
Θ_a	$\ln A_0 + \frac{\sigma_a^2}{2\kappa_a}$
σ_a	0.8
λ^a_{idio}	5
μ^a_{idio}	0
σ^a_{idio}	0.3
λ_{syst}	2
μ_{syst}	0
σ_{syst}	0.3

Table 2: Parameter setting used for the simulation of crypto assets for the analysis of the stability mechanism (see Section 5).

4.2.3 Simulating Non-Celo Reserve Assets

For the scenario generation of crypto assets we follow a similar approach as for the scenario generation of the demand quantity. With the parameter setting of the crypto asset processes we are trying to take into account the requirements for the scenario generation that we have outlined in Section 2. It is our intention to create a wide range of plausible scenarios that include steep downturns as well as upturns and to take into account scenarios that expose the stability mechanism to the stability risks outlined in Section 1.2.

Model Choice: We choose a geometric Ornstein-Uhlenbeck process with jumps from a compound Poisson process for the scenario generation (see Section 2.2). The reasons are discussed in Section 2 (see Appendix A for a more technical discussion).

Parameter Setting: At first we would like to set the drift parameter Θ_a such that 50% of the paths are above and 50% are below the initial value. By rearranging Equation (68) and using $p_{\mathcal{N}}(50\%) = 0$, the drift parameter Θ_a can be expressed as a function of κ_a, σ_a and the target value at time t

$$\Theta_a = \frac{1}{1 - e^{-\kappa_a t}} \left(\ln \text{ target} - e^{-\kappa_a t} \ln A_0 \right) + \frac{\sigma_a^2}{2\kappa_a} \ . \tag{13}$$

Our target value is the initial value target $= A_0$. Therefore the drift parameter Θ_a is given by

$$\Theta_a = \ln A_0 + \frac{\sigma_a^2}{2\kappa_a} \ . \tag{14}$$

Crypto markets exhibit a comparably high volatility; annualised volatilities[7] around 1 or significantly above 1 are common. We use the magnitude of the observed volatilities to have a rough estimate. As the percentiles of the process scale with the parameter σ_a, i. e. larger σ_a values create wider percentiles (see Equation (68)), the final parameter is ultimately set such that it yields sufficiently wide percentiles. With the final parameter setting (see Table 2) the ranges limited by the 5th and 95th and the 1st and 99th percentile at $t = 30$ years are approximately $[1 \times 10^{-5}, 7 \times 10^4]$ and $[8 \times 10^{-8}, 8 \times 10^6]$. Figure 6 shows the evolution of a few percentiles obtained with the same parameter setting.

The mean reversion parameter κ_a has influence on how fast the percentiles become constant which prevents the decay and divergence that can occur with geometric Brownian motions (see Section 2). In the case of the specific parameter setting of the drift parameter θ (constant 50th percentile) we do not really require this feature of the geometric Ornstein-Uhlenbeck process. Hence, we set the mean reversion speed to a low value $\kappa_a = 0.001$.

The process of a crypto asset both has an idiosyncratic and a systematic jump component. For both components we follow the idea of the heuristic 3σ rule according to which events that deviate more than three standard deviations from the mean are considered to be an outlier. With a volatility

[7] Standard deviation of log-returns

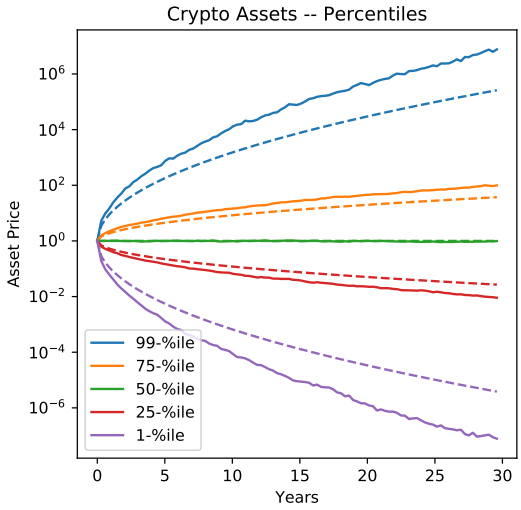

Figure 6: This figure shows empirical percentiles (sample size = 10 000) of the crypto asset process using the parameter settings summarised in Table 2. As a reference the dashed lines show the theoretical percentiles of a geometric Ornstein-Uhlenbeck process without jumps. At each time t, 50% of the paths are above the initial value and 50% of the paths are below the initial value.

parameter of $\sigma_a = 1$, we set the volatility parameter of the idiosyncratic and the systematic jump size variable $\sigma^a_{idio} = 0.3$. We have obtained this value by rounding down $6\frac{\sigma_d}{\sqrt{360}} = \frac{6}{\sqrt{360}}$, i.e. six times the daily volatility $\frac{\sigma_d}{\sqrt{360}}$. In the case of a normal distribution, an event of larger or equal to 3σ occurs with probability 0.3%, which would be approximately once in 360 days. We set the jump intensity of the idiosyncratic Poisson process $\lambda^a_{idio} = 5$ to have five additional idiosyncratic events per year on average and the jump intensity of the systematic Poisson process $\lambda_{syst} = 2$ to have two additional systematic events. The jump process leads to an additional widening of the percentiles. This can been seen in Figure 6 by comparing the solid lines with the dashed lines.

To model the correlation ρ_{a_i,a_j} between crypto assets, we assume that the returns of the reserve assets follow a single factor structure, as per [3]:

$$R_t = \beta f_t + \epsilon_t \tag{15}$$

$$\text{with} \quad f_t \sim \mathcal{N}\big(\mu_f, \sigma_f^2\big) \quad \text{and} \quad \epsilon_t \sim \mathcal{N}(0, \Sigma_\epsilon)$$

where μ_f and σ_f^2 influence the average of the drift parameters and the average of the variance of the assets respectively. Σ_ϵ gives the covariance matrix of the error terms and is assumed to be diagonal with volatilities drawn from a uniform distribution with a specific support $[\sigma_{\epsilon,l}, \sigma_{\epsilon,u}]$. The elements of β are spread evenly between 0.5 and 1.5.

DeMiguel [3] chose the parameters μ_f, σ_f, $\sigma_{\epsilon,l}$ and $\sigma_{\epsilon,u}$ such that the resulting moments are aligned with empirically observed equity returns. For our purposes, we would like to be able to choose different sets of parameters that capture a range of possible future scenarios. We do so by adjusting the DeMiguel approach such that it allows us to specify an average mean return and an average volatility, and then extrapolate the mean return vector and covariance matrix given those inputs. The implementation used in this version of the stability analysis assumes $N = 10$ assets in the reserve.

4.2.4 Pricing Celo native asset

To price the Celo portion of the reserve, we must come up with a pricing model for CELO. The pricing model we derive in this section is an effort to demonstrate potential outcomes in a stability analysis, and are not intended to show or suggest that CELO will appreciate in value.

Like in pricing models for actual gold or other traditional reserve assets, we assume that there are multiple components to the value of CELO. In our case, we assume two: the first, which we call the expansion value, is based on the protocol-directed purchases of CELO when the demand

for Celo Dollars increases. The second, which we call the utility value, is based on the fact that transaction fees on the Celo network can be paid in CELO.

We also assume that the market participants, which in aggregate hold all floating CELO at time point t, expect their CELO ownership to be diluted over time - for example by block rewards and reserve transactions. More precisely, we assume that the ownership fraction ω_t for $u \geq t$ can be described as

$$\omega_t(u) = \omega \exp(-\nu(u-t)) \tag{16}$$

with $\omega = 1$, $\nu > 0$ and where ν denotes the fraction of annual ownership dilution.

4.2.4.1 Expansion Value

The *expansion value*, qualitatively, derives from the fact that, on expansion in demand for Celo Dollars, the protocol will purchase CELO.

Assume that market participants observe a Celo Dollar demand Q_t at time t and that, for simplicity, they anticipate a Celo Dollar demand growth with a rate of $\hat{\mu} \geq 0$ (no uncertainty). Also assume that the demand at 1 US Dollar at time t equals the supply, i.e. $Q_t = S_t$, and that the protocol can be expected to match supply to demand. The Celo Dollar demand $\hat{Q}_t(u)$ and supply $\hat{S}_t(u)$ at a future time u with $u > t$ anticipated[8] by market participants at time $t < u$ who are observing the demand Q_t is given by:

$$\hat{Q}_t(u) = Q_t \exp(\hat{\mu}(t-s)) \quad \text{and} \quad \hat{S}_t(u) = S_t \exp(\hat{\mu}(t-s)) \ . \tag{17}$$

The anticipated demand $\hat{Q}_t(u)$ and supply $\hat{S}_t(u)$ are calculated for every simulated time point s along each simulation path k, i.e. formally we would need another index (e.g. Q_t^k and $\hat{Q}_t^k(u)$). However, we drop the path index k for the sake of simplicity and assume that all the following formulas are defined for every individual path. The expected instantaneous expansion of supply is thus

$$d\hat{S}_t(u) = \hat{\mu} S_t(u) du. \tag{18}$$

In this model, the present value at time t generated through future expansions, V_t^e, can be calculated by integrating over the product of the expected fractional ownership and the discounted expansion amounts

$$V^e(t) = \int_t^\infty \omega_t(u) \exp(-r(u-t)) \, \hat{\mu} S_t \exp(\hat{\mu}(u-t)) \, du \ . \tag{19}$$

where r is the discount rate. Evaluating this integral

$$V_t^e = \frac{\hat{\mu} S_t}{\hat{\mu} - r - \nu} \left[\exp\left[(\hat{\mu} - r - \nu)(u-t) \right] \right]_t^\infty \tag{20}$$

under the assumption $r + \nu > \hat{\mu}$ gives

$$V_t^e = \frac{\hat{\mu}}{r + \nu - \hat{\mu}} S_t \ . \tag{21}$$

If an annual stability fee of size s is introduced, then this increases the necessary expansion rate from $\hat{\mu}$ to $\hat{\mu} + s$ and thus leads to an expansion value of CELO of

$$V_t^e = \frac{\hat{\mu} + s}{r + \nu - \hat{\mu} - s} S_t \tag{22}$$

The derivation of this result can be seen as a variation of the Gordon Growth model [4]. If one for example assumes positive Celo Dollar demand growth of 5%, a 10% ownership dilution, a 0.5% stability fee and a discount rate of 25%, than a multiplier $\frac{V_t^e}{S_t} = 0.1864$ results. If we assume zero growth in Celo Dollar demand, i.e. $\hat{\mu} = 0$, Equation (22) would reduce to

$$V_t^e = \frac{s}{r + \nu - s} S_t \tag{23}$$

which leads to a ratio of $\frac{V_t^e}{S_0} = 0.0145$.

[8] The stochastic process Q_t is unknown to the market participants. As part of their purchasing decision they form an opinion about the future growth given a currently observable demand Q_t. Therefore, the demand $\hat{Q}_t(u)$ anticipated by the market participants is not the same as the expectation value $\mathbb{E}[Q_t]$.

4.2.4.2 Utility Value

The *utility value* of CELO derives from the fact that transaction fees are paid in CELO[9]. If Celo Dollar holders pay a transaction fee f for each transaction, the incremental fee is:

$$dF_s(u) = vf\hat{S}_t(u)du. \tag{24}$$

where v is the annual velocity of Celo Dollars.

Just as in the calculation of the expansion value, the utility value follows from integrating over the product of the expected fractional ownership and the discounted expected future inflows:

$$V_t^u = \int_t^\infty \omega_u \exp(-r(u-t))\, vfS_t \exp(\hat{\mu}(u-t))\, dt. \tag{25}$$

Evaluating this integral

$$V_t^u = \frac{vfS_t}{\hat{\mu} - r - \nu} \left[\exp\left[(\hat{\mu} - r - \nu)\, u\right]\right]_t^\infty \tag{26}$$

under the assumption that $r + \nu > \hat{\mu}$ results in a utility value of:

$$V_t^u = \frac{vf}{r + \nu - \hat{\mu}} S_t. \tag{27}$$

4.2.4.3 Modeling CELO Downward Pressure

To account for potential downward pressure on the value of CELO in times in which the Celo reserve is critically low, we model a value multiplier M^g that reduces the total value of floating CELO as a function of the crypto-reserve-ratio rr_c, that is the total stable token supply over the value of the non-Celo part of the crypto reserve. This multiplier is modeled as a piece-wise linear function as follows

$$M_t^g = \begin{cases} 1 & \text{if } rr_t^c \geq \tau^g \\ \frac{rr_t^c}{\tau^g} & \text{if } 0 \leq rr_t^c < \tau^g \end{cases}. \tag{28}$$

The simulations conducted in this analysis assume $\tau^g = 0.5$. This implies that the value of CELO is discounted as soon as the value of the non-Celo part of the Celo crypto reserve drops below a level at which it could cover 50% or less of the total stable token supply.

The above multiplier can lead to downward spirals in the value of the CELO reserve as a drop in the value of CELO leads to a reserve rebalancing in which more CELO is bought via non-Celo crypto assets. This reduces the crypto-reserve-ratio, which in times of a already low crypto-reserve-ratio decreases the multiplier, which reduces the value of the CELO reserve further and so forth. The downward spiral effect is especially pronounced when a similar multiplier is introduced for the Celo Dollar demand. Such a multiplier is also employed in this analysis and was introduced in Section 3.3.

4.2.4.4 Total Value and Price

The total value V_t of CELO in float is calculated as the sum of the expansion and the utility value adjusted by the downward pressure multiplier:

$$V_t = M_t^g \left(V_t^e + V_t^u\right). \tag{29}$$

Additionally, we assume a lower bound on the total value of CELO in float of 3/2 of the value of the non-Celo reserve as buying up 2/3 of the floating CELO would allow an individual to gain control over the proof-of-stake network and therefore the non-Celo reserve. Future versions of this article might account for potential additional value drivers of CELO, like a governance token value and a value derived from expected future reserve rebalancings, and will refine the pricing model used in this article

[9]Transaction fees may also be paid in Celo Dollars. Therefore, part of the value derived from transaction fees could be counted towards the expansion value since Celo Dollar-denominated transaction fees can be expected to increase the demand for Celo Dollars. Stability should not be fundamentally affected by this and we will model the Celo Dollar-denominated transaction fee scenario explicitly in a future version of this paper.

Once we have the total value V_t of CELO in float at time t, we can compute the price p_t of a single CELO coin as follows:

$$p_t = \frac{V_t}{G_t}. \tag{30}$$

where G_t is the quantity of CELO in float at time t (not counting CELO in the reserve). In our model, the number of coins in the reserve and float is known at any time t, and so we can use p_t to derive a value of the CELO portion of the reserve at time t.

4.2.5 Additional Mechanisms to Bolster the Reserve

In addition to the natural price dynamics of the reserve, two additional mechanisms serve to bolster the reserve.

4.2.5.1 Block Reward Distribution Scheme

On Celo, a fraction of the epoch rewards is distributed to the reserve during times in which the reserve ratio is below a certain threshold. This threshold is modeled as a linear function, decreasing from 2 to 1 over the course of 25 years. The simulation assumes that 25% of the epoch rewards, i.e. the fraction that would be distributed to the community fund during normal times, are redirected to the reserve if this threshold is crossed.

4.2.5.2 Reserve Fee

For every trade with the Celo reserve exchange, the reserve charges a small percentage fee ρ. All proceeds from this fee go towards bolstering the reserve.

4.3 Constraints to Adjusting Supply: Liquidity

Even during times of a sufficiently large reserve, depegs can occur if there are liquidity related frictions during expansions and contractions of Celo Dollar supply. This section describes the Celo expansion and contraction mechanism, called CP-DOTO and the liquidity related risks this mechanism faces. It then describes how these risks are modelled in this analysis.

4.3.1 The Constant-Product Decentralized One-to-One Mechanism (CP-DOTO)

At a high level, the Celo expansion and contraction mechanism allows users to create new Celo Dollars by sending 1 US Dollar worth of CELO to the reserve, or to burn Celo Dollars by redeeming them for 1 US Dollar worth of CELO(decentralized one-to-one mechanism (DOTO)). In order for a user to send 1 US Dollar worth of CELO to the reserve, or redeem 1 US Dollar worth of CELO from the reserve, the protocol needs an oracle to give the exact price of CELO in US Dollars. In cases where the CELO to US Dollar oracle value is imprecise (in other words, if CELO is trading on the market at a different price than what the oracle reports), arbitrage opportunities exist even if the Celo Dollar is perfectly pegged[10]. These unintended arbitrage opportunities can lead to unintended supply adjustments and reserve depletion. The next section describes the implementation of the above mechanism that mitigates this potential.

To address the risk of imprecise oracle values for the CELO to US Dollar exchange rate in the DOTO mechanism, the protocol uses a constant-product market-maker model (CP), inspired by Uniswap (see [12]), to dynamically adjust the on-chain exchange rate in response to on-chain exchange activity. For that purpose, two wallets controlled by the protocol, one containing Celo Dollars and one containing CELO, are initialized whenever the oracle value is updated. Let $G^r(t_0)$ denote the number of CELO coins and $C^r(t_0)$ the number of Celo Dollar coins in the respective wallets at initialization. The central equation for the constant-product market-maker model fixes the following relationship:

$$G^r(t_0) \times C^r(t_0) = G^r(s) \times C^r(s) \qquad \forall \quad t_0 \leq s < t_1 \ , \tag{31}$$

[10]To give a concrete example, if the oracle reports the price of CELO as \$1.50, and CELO is trading on the open market for \$2, then users have an incentive to redeem their Celo Dollars for CELO from the reserve at \$1.50 and then sell the CELO on the open market for \$2. Further, in that scenario, nobody would buy Celo Dollars from the reserve, because they will need to pay \$2 worth of CELO to buy 1.50 Celo Dollars.

where t_1 denotes the point in time of the next oracle value update.

Given this, it can be shown (see [12]) that the price for an infinitesimal amount of CELO in Celo Dollar units in the period $t_0 \leq s < t_1$ is

$$P_s = \frac{C^r(s)}{G^r(s)} \ . \tag{32}$$

Whenever the oracle price of CELO is updated, the protocol initializes wallet quantities $C^r(t)$ and $G^r(t)$ that lead to a on-chain price P_t which equals the current oracle rate.

If the oracle price is correct, the exchange rate quoted by the constant-product market-maker will be equal to that of the market, and no arbitrage opportunity will exist if the Celo Dollar is pegged. If the oracle price is incorrect, the two rates will differ, and an arbitrage opportunity will exist even in the absence of a Celo Dollar depeg. As arbitrageurs exploit this opportunity the constant-product market-maker model will dynamically adjust the quoted exchange rate until the arbitrage opportunity ceases to exist. This limits the depletion potential of the Celo expansion and contraction mechanism in the case of an incorrect oracle price.

In this analysis, we take the conservative approach of assuming that no external market makers or other market participants are willing to compensate short-term fluctuation of the Celo Dollar at market places on their own account. The short-term price fluctuations resulting in this simulation analysis are thus a conservative estimate of the short-term stability of the Celo Dollar.

4.3.2 Modeling CP-DOTO Interactions

In this section we are providing an analytical discussion of the mechanics of CP-DOTO for a specific market setup. First we describe the setup and its assumptions. This is followed by a summary of the key outcomes of the analysis. The formal results behind those outcomes and their proofs can be found in Appendix B. The parameters used in the examples discussed below are provided in Table 3.

4.3.2.1 Model Setup

The model setup can be decomposed into two components: the on-chain market and the open market. Both components are illustrated in Figure 7. As described in Section 4.3.1 the on-chain market is following the CP-DOTO mechanism. The on-chain price of CELO at time t quoted in Celo Dollar is denoted by P_t. On-chain Celo Dollar and CELO are represented by wallets. We denote the amount of Celo Dollar and CELO in each wallet at time t by $C^r(t)$ and $G^r(t)$, respectively. At the time of an oracle update t the amount of CELO $G^r(t)$ is chosen as a fraction ϕ^r of the CELO amount in the reserve

$$G^r(t) = \phi^r \times \text{Reserve CELO} \tag{33}$$

and the Celo Dollar amount is set to

$$C^r(t) = P_t G^r(t) \ . \tag{34}$$

Due to the constant-product market maker the following equation is satisfied at all times s and t within one oracle update cycle:

$$C^r(s)G^r(s) = C^r(t)G^r(t) \ . \tag{35}$$

For the open market we are considering Celo Dollar, CELO and US Dollar each represented by a hypothetical tank with tank size $C^m(t)$, $G^m(t)$ and $U^m(t)$. We denote the market prices by $X^c_g(t)$, $X^u_g(t)$ and $X^u_c(t)$. This convention follows the rule that a symbol 'X' denotes the price of currency in sub-script quoted in the currency in super-script. We are assuming that all arbitrage opportunities within the currency triangle of the open market will immediately vanish due to arbitrage trading. In particular, we are assuming

$$X^u_c(t) = X^u_g(t)X^g_c(t) \ , \quad X^u_c(t) = \frac{1}{X^c_u(t)} \ , \quad X^u_g(t) = \frac{1}{X^g_u(t)} \ , \quad \ldots \tag{36}$$

Tank sizes and market prices are related by the assumption that the relative sizes of the tanks are given by:

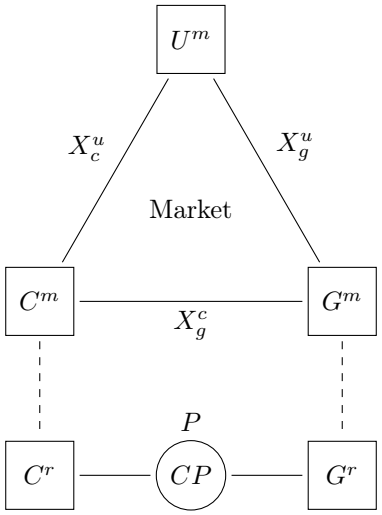

Figure 7: The diagram illustrates the model setup. It shows the three market tanks C^m, G^m and U^m and the market prices X_g^c, X_g^u and X_c^u. Below the market currency triangle, CP-DOTO is represented by the two wallets C^r and G^r. On-chain transactions (Celo Dollar $\leftrightarrow$ CELO) are determined by the constant-product market maker (CP) at a price P. The dashed lines indicate transfers with the open market and the on-chain CP-DOTO mechanism.

$$\frac{C^m(t)}{G^m(t)} = X_g^c(t) \ , \quad \frac{U^m(t)}{G^m(t)} = X_g^u(t) \quad \text{and} \quad \frac{U^m(t)}{C^m(t)} = X_c^u(t) \ . \tag{37}$$

For every transaction with CP-DOTO a relative fee ρ will be applied. If M Celo Dollars are transferred ρM Celo Dollars will be burned and effectively $(1-\rho)M$ Celo Dollars will reach CP-DOTO, if M CELO tokens are transferred to CP-DOTO ρM CELO tokens will be send to the reserve and effectively $(1-\rho)M$ CELO tokens will reach CP-DOTO.

Under the assumption that the Celo Dollar price has deviated from the peg it follows that the CELO price quoted in US Dollar $X_g^u(t)$ is different from the CELO price quoted in Celo Dollar $X_g^c(t)$

$$1 \neq X_c^u(t) = X_g^u(t) X_c^g(t)) = \frac{X_g^u(t)}{X_g^c(t)} \quad \Leftrightarrow \quad X_g^u(t) \neq X_g^c(t) \ . \tag{38}$$

By construction, at time t of an oracle update the on-chain CELO price P_t (quoted in Celo Dollar) is equal to the market CELO price $X_g^u(t)$

$$P_t = X_g^u(t) \ . \tag{39}$$

Therefore, the on-chain CELO price P_t is different from the market CELO price $X_g^c(t)$

$$P_t \neq X_g^c(t) \ . \tag{40}$$

From the perspective of arbitrage traders two cases are profitable:

1. $(1-\rho)X_g^c(t) > P_t$ which is equivalent to $X_c^u(t) = X_g^u(t)X_g^c(t) < 1-\rho$
2. $X_g^c(t) < (1-\rho)P_t$ which is equivalent to $X_c^u(t) = X_g^u(t)X_g^c(t) > \frac{1}{1-\rho}$.

In both cases we are assuming that arbitrage traders will take advantage of the arbitrage opportunity until it vanishes at time t_e, i.e. until either $(1-\rho)X_g^c(t_e) = P_{t_e}$ or $X_g^c(t_e) = (1-\rho)P_{t_e}$. We refer to each of these states as the equilibrium state.

In the first case the equilibrium state is described by the following set of equations of unknown time t_e quantities:

$$(1-\rho)X_g^c(t_e) = P_{t_e} \tag{41}$$
$$C^r(t_e)G^r(t_e) = C^r(t)G^r(t) \tag{42}$$
$$C^r(t_e) + C^m(t_e) + \rho(C^m(t) - C^m(t_e)) = C^r(t) + C^m(t) \tag{43}$$
$$G^r(t_e) + G^m(t_e) = G^r(t) + G^m(t) \ . \tag{44}$$

The set of equations can be solved to give solutions with regard to time t quantities (see Appendix B for details). We state the CELO price P_{t_e} and the Celo Dollar price $X_g^u(t_e)$

$$P_{t_e} = \frac{C^r(t) + (1-\rho)C^m(t)}{G^r(t) + G^m(t)} \tag{45}$$

$$X_g^u(t_e) = \frac{U}{C^m(t_e)} = \frac{U}{\frac{1-\sqrt{\frac{P_t}{P_{t_e}}}}{1-\rho} C^r(t) - C^m(t)} \ . \tag{46}$$

In the second case the equilibrium state is described by a similar set of unknown time t_e quantities:

$$X_g^c(t_e) = (1-\rho)P_{t_e} \tag{47}$$

$$C^r(t_e)G^r(t_e) = C^r(t)G^r(t) \tag{48}$$

$$C^r(t_e) + C^m(t_e) = C^r(t) + C^m(t) \tag{49}$$

$$G^r(t_e) + G^m(t_e) + \rho(G^m(t) - G^m(t_e)) = G^r(t) + G^m(t) \ . \tag{50}$$

The set of equations can be solved to give solutions with regard to time t quantities (see Appendix B for details). We state the CELO price P_{t_e} and the Celo Dollar price $X_g^u(t_e)$

$$P_{t_e} = \frac{C^r(t) + C^m(t)}{G^r(t) + (1-\rho)G^m(t)} \tag{51}$$

$$X_g^u(t_e) = \frac{U}{\left(1 - \sqrt{\frac{P_t}{P_{t_e}}}\right) C^r(t) - C^m(t)} \ . \tag{52}$$

4.3.2.2 Major CP-DOTO Properties

In this section we are discussing the key observations about CP-DOTO applied to the theoretical model setup described above. All observations have to be considered as statements that are only true within this model setup. They cannot be directly transferred to real market situations. However, they help to gauge expectations of the effect of CP-DOTO.

Approaching the peg

After one arbitrage cycle has been completed, on-chain and open market CELO prices P_{t_e} and $X_g^c(t)$ are equal apart from the fee related spread:

$$(1-\rho)X_g^c(t_e) = P_{t_e} \quad \text{or} \quad X_g^c(t_e) = (1-\rho)P_{t_e} \ . \tag{53}$$

Even though on-chain and open market CELO price are equal, the Celo Dollar price $X_c^u(t)$ will not reach the target price exactly after a single step in this model (even if the fee is set to $\rho = 0$). The intuitive reason for this behaviour is that the arbitrage cycle affects both open market tank sizes (Celo Dollar and CELO) representing the CELO price $X_g^c(t)$ in inverse directions simultaneously. But it only affects one market tank size (Celo Dollar) representing the Celo Dollar price quoted in US Dollar $X_c^u(t)$.

In order to reach the peg, multiple oracle updates must be performed. This means after an update of the on-chain price $P_{t_1} := X_u^c(t_1)$ arbitrage trading through CP-DOTO leads to an equilibrium state at time t_{e_1}: On-chain and open market CELO prices are equally apart from the fee related spread. The Celo Dollar price $X_c^u(t_{e_1})$, however, has not reached the exact peg yet. Therefore, the on-chain CELO price is updated and set to the open market CELO price quoted in US Dollar $P_{t_2} := X_u^c(t_2)$. After the update a new arbitrage cycle starts. By repeating the oracle update, the Celo Dollar price is converging towards the peg. In Figure 8 the evolution of the three market prices is shown under multiple oracle update and arbitrage cycles. It should be pointed out that this model does not take other market participants into account who form expectations of the price and trade accordingly. Accounting for such actors could speed up the process of price convergence further.

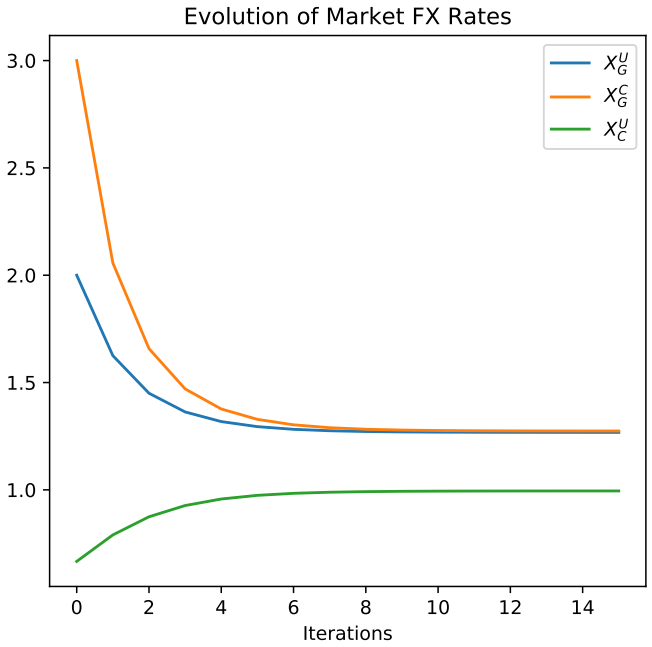

Figure 8: Evolution of prices for multiple oracle update iterations. With each iteration, the Celo Dollar price $X_c^u(t)$ moves closer to the target.

Benefit of high on-chain liquidity

The on-chain and open market price in the equilibrium state at time t_e ranges between the initial on-chain and open market prices at time t:

$$X_g^u(t) = P_t < P_{t_e} < (1-\rho)X_g^c(t) \quad \text{or} \quad \frac{1}{(1-\rho)}X_g^c(t) < P_{t_e} < P_t = X_g^u(t)\ . \tag{54}$$

The position of CELO price within this range depends on the size of the on-chain wallet sizes in comparison to the open marked tank sizes. The larger the tank sizes in comparison to the open market tank sizes($G^r(t)$ vs. $G^m(t)$ or $C^r(t)$ vs. $C^m(t)$), the closer the price at equilibrium P_{t_e} will be to the oracle value $P_t = X_g^u(t)$ and vice versa.

The impact of the on-chain tank size on the convergence speed of the Celo Dollar price $X_c^u(t)$ is illustrated in Figure 9. Two relative sizes of the on-chain CELO wallet and the market CELO tank are analysed.[11] The blue line in Figure 9 has been created with an initial relative tank size of $\frac{G^m(t_0)}{G^r(t_0} = 50\%$ and the orange line with an initial relative tank size of $\frac{G^m(t_0)}{G^r(t_0} = 5\%$. The large relative tank size results in a faster convergence of the Celo Dollar price towards 1.

Drawback of high on-chain liquidity

Malicious attacks that target the oracle value can be used to deplete the reserve by enforcing artificial arbitrage opportunities that lead to a net outflow of CELO from the on-chain wallet into the market. In Figure 10a the cumulative CELO outflow from the on-chain wallet into the open market is shown in the case of an attack that updates the on-chain CELO price $P_t := \frac{1}{5}X_g^u(t)$ with 20% of the true market CELO price $X_c^u(t)$ in every update and arbitrage cycle. To capture the effect on the CELO reserve the cumulative amount of CELO transferred from the on-chain wallet to the open market is shown. Two different settings with regard to the size of the on-chain CELO wallet (10% or 0.1% of the CELO amount in the reserve) are analysed. In Figure 10a the net outflow into the market after 100 iterations is equal to the reserve amount of 100m CELO; the reserve has been depleted. In Figure 10b the net outflow after 100 iterations is only 6m. The larger wallet size (reserve fraction of 10%) leads to a higher speed of CELO outflow.

The faster depletion in the case of larger on-chain tanks has two reasons. Firstly, the size of the on-chain CELO tank is a natural bound for the amount of CELO that can be transferred to the

[11] The on-chain tank size is kept constant and the market tank size is adjusted.

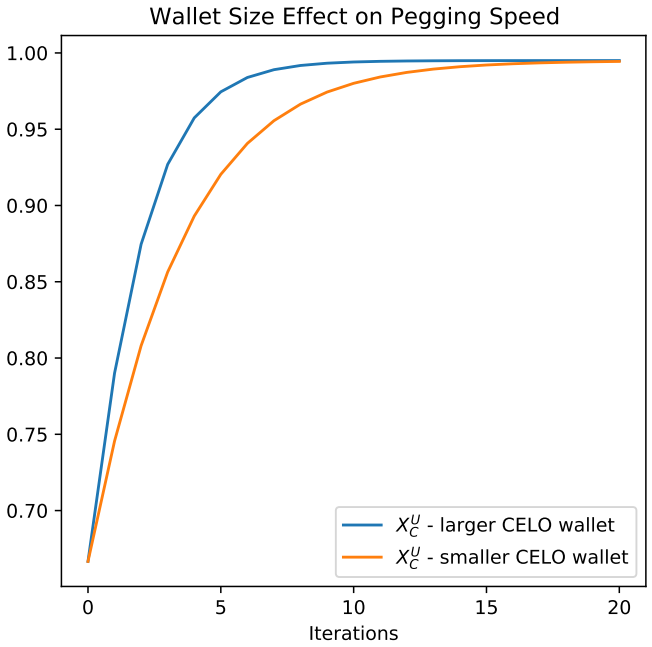

Figure 9: Two relative sizes of the on-chain CELO wallet and the market CELO tank are analysed. The blue line in Figure 9 has been created with an initial relative tank size of $\frac{G^m(t_0)}{G^r(t_0} = 50\%$ and the orange line with an initial relative tank size of $\frac{G^m(t_0)}{G^r(t_0} = 5\%$. The large relative tank size results in a faster convergence of the Celo Dollar price towards 1.

open market within on cycle. Secondly, due to the pricing effect of the constant product market maker, the same amount of CELO is cheaper the larger the on-chain tanks are.

4.3.3 CP-DOTO Parameter Settings

In this simulation analysis, we modeled that the CP-DOTO oracle is updated 24 times per day ($f_{update} = \frac{1}{24}$) and that a representative agent takes the resulting arbitrage opportunities after every update such that the equilibrium (including the new Celo Dollar supply) described in Appendix B is reached. The CELO tank is set to $\phi^r = 10\%$ of the total amount of CELO in the reserve after every oracle update following Equation (33). Subsequently, the Celo Dollar tank size is chosen in accordance with Equation (34) such that the CP-DOTO price P_t reflects the reported oracle value. The CP-DOTO fee is set to $\rho = 0.005$. The resulting Celo Dollar supply after the 24 daily updates is used to derive the end-of-day Celo Dollar price in the simulated time step via the demand curve model described in Equation (9).

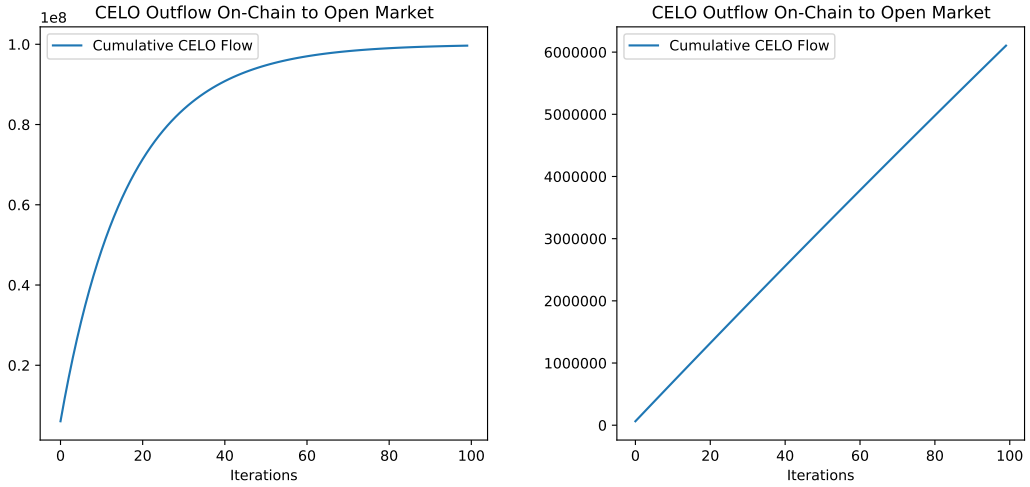

(a) Reserve Fraction 10%

(b) Reserve Fraction 0.1%

Figure 10: Assume the oracle feed is under a malicious attack. Instead of the true CELO market price $X_g^u(t)$ the value $\frac{1}{5}X_g^u(t)$ is used to update the on-chain price $P_t := \frac{1}{5}X_g^u(t)$. To capture the effect on the CELO reserve the cumulative amount of CELO transferred from the on-chain wallet to the open market is shown. Two different settings with regard to the size of the on-chain CELO wallet (10% or 0.1% of the CELO amount in the reserve) are analysed. In Figure 10a the net outflow into the market after 100 iterations is equal to the reserve amount of 100m CELO; the reserve has been depleted. In Figure 10b the net outflow after 100 iterations is only 6m. The larger wallet size (reserve fraction of 10%) leads to faster CELO outflows.

5 Simulation Results

Using the stochastic models for Celo Dollar demand and the crypto market, as well as the model of supply adjustments via interactions with CP-DOTO, we analyzed the price stability of the Celo Dollar by simulating a wide range of possible scenarios.

Table 4, which can be found in Appendix 5, gives a collective overview over the parameter setting for which we simulated 100,000 paths. Each path has daily time steps and simulates a period of 30 years assuming 360 days per year. This gives a total of 1.08 Billion simulated days in which the supply adjustments to changes in Celo Dollar demand are calculated.

Figure 11 focuses on the depeg scenarios by showing 0.1% and 0.01% percentiles of the simulated Celo Dollar price paths. The figure indicates that there is a non-zero chance of a permanent depeg of the Celo Dollar price but the relative frequency of such permanent depegs is very low in our simulation model as they only show in these percentiles. The occurrence of these permanent depegs are directly related to the downward spirals modeled as described in Sections 3.3 and 4.2.4.3. In these paths, a very negative crypto market evolution in combination with a strong decrease in Celo Dollar demand reduces the crypto-reserve-ratio so that a downward pressure eventually leads to a permanent depeg. For order of magnitude one could compare the percentiles of the depeg scenarios to historic credit events. While these are different distributions, and data for the likelihood of a default over a particular time horizon is not widely available, some research exists on the historic default rates of bonds with a credit rating. Based on the Standard & Poor's Global Report ([11]) the global average cumulative default rate from 1981-2017 for a AAA rated bond is 0.13% over 3 years and 0.24% over 4 years.

Figure 12 shows 1% up to 99.99% percentiles for the Celo Dollar price for every day of the simulated 30 year period. It can be seen that the Celo Dollar price closely tracks the price of 1 US Dollar for the vast majority of the simulated paths. Fluctuations around 1 US Dollar are slightly larger in the first few years than later into the 30 years period but large deviations are rare under the modeling assumptions made in this article.

All results shown and discussed in this section must be seen in light of the modeling assumptions, parameter choices and general limitations of this simulation analysis. Many of the parameter choices are necessarily subjective and the chosen protocol parameters might not coincide with the

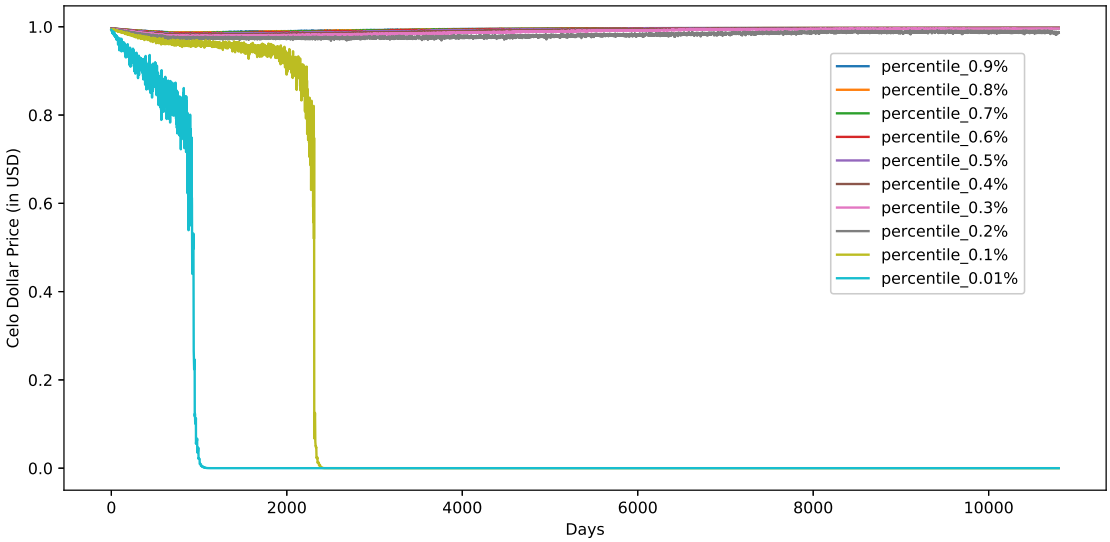

Figure 11: Depeg scenarios: Per-day Celo Dollar price percentiles in USD, 0.9% to 0.01%, for every day across the simulated 30 year period. Such permanent depegs occur with very low relative frequency in our simulation model given the chosen parameters.

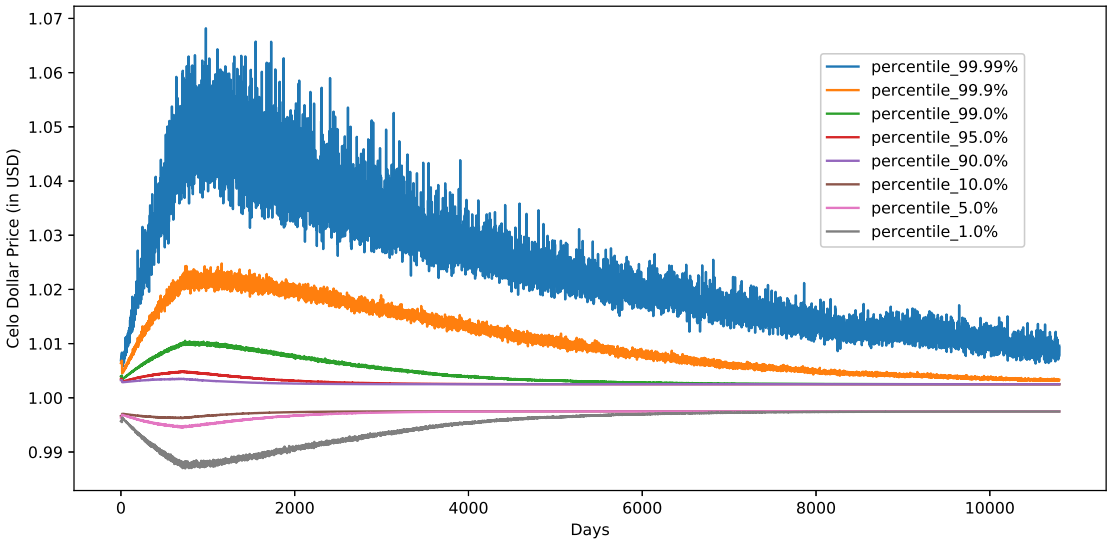

Figure 12: Per-day Celo Dollar price percentiles in USD, 1% to 99.99%, for the simulated 30 year period.

parameters at launch of the Celo network. Also, additional actors like external liquidity providers could have significant influence on stability. Risk diversification of the Celo reserve can be expected to be of central importance for Celo Dollar price stability and as the crypto asset market matures, additional low-volatility and tokenized assets classes might become available which could help with further diversifying the risk of the reserve.

6 Conclusion

The purpose of this analysis is to gain a better understanding of the stability-related mechanics of the Celo protocol. Future versions of the analysis will continue to refine the Celo Dollar demand and supply adjustment models. Further, in future versions we plan to model large scale adversarial attacks, and include additional features of the protocol that we did not include in the current version, for example by introducing multiple stable value assets.

All results in this analysis must be taken with caution as they are derived under specific modeling assumptions and parameter choices. Modeling certain features differently and/or choosing different parameter settings will necessary lead to different results.

References

[1] Nader Al-Naji, Josh Chen, and Lawrence Diao. Basis: A price-stable cryptocurrency with an algorithmic central bank. 06 2018.

[2] Stephen Chan, Jeffrey Chu, Saralees Nadarajah, and Joerg Osterrieder. A statistical analysis of cryptocurrencies. *Journal of Risk and Financial Management*, 10:12, 05 2017.

[3] Victor DeMiguel, Lorenzo Garlappi, and Raman Uppal. Optimal versus naive diversification: How inefficient is the 1/N portfolio strategy? *Review of Financial Studies*, 22(5):1915–1953, 2009.

[4] M.J Gordon and Eli Shapiro. Capital Equipment Analysis: The Required Rate of Profit. *Management Science*, 3(1):102–110, 1956.

[5] Sep Kamvar, Marek Olszewski, and Rene Reinsberg. Celo: A Multi-Asset Cryptographic Protocol for Decentralized Social Payments, 2018.

[6] John L. Kelly. A new interpretation of information rate. *Bell System Technology Journal*, 35:917–926, 1956.

[7] Harry Markowitz. Portfolio Selection. *The Journal of Finance*, 7(1):77–91, 1952.

[8] Robert Michaud. Efficient Asset Management. *Boston: Harvard Business School Press*, 1998.

[9] Nicholas Platias and Marco Di Maggio. Terra money: Stability stress test. 05 2019.

[10] Jan Jakub Szczygielski, Andreas Karathanasopoulos, and Adam Zaremba. One shape fits all? a comprehensive examination of cryptocurrency return distributions. *Applied Economics Letters*, 0(0):1–7, 2019.

[11] Diane Vazza, Nick W Kraemer, and Evan M Gunter. 2018 Annual Global Corporate Default And Rating Transition Study. Technical report, Standard & Poors, 2019.

[12] Yi Zhang, Xiaohong Chen, and Daejun Park. Formal Specification of Constant Product (x × y = k) Market Maker Model and Implementation. 2018.

Appendix

A Scenario Generation

A.1 Regimes of the Geometric Brownian Motion

In this section we discuss a specific property of the geometric Brownian motion that depending on the requirements can be unsuitable for the generation of scenarios. First, we state this property in a rather formal manner and provide a more intuitive explanation afterwards.

A geometric Brownian motion satisfies the following stochastic differential equation

$$dX_t = \mu X_t dt + \sigma X_t dW_t \ , \tag{55}$$

where W_t is a Brownian motion, μ is the drift parameter and σ the volatility parameter. The solution is given by

$$X_t = X_0 \exp\left((\mu - \frac{1}{2}\sigma^2)t + \sigma W_t\right) \ . \tag{56}$$

X_t is log-normally distributed

$$X_t \sim \log\mathcal{N}\left((\ln X_0 + (\mu - \frac{1}{2}\sigma^2)t,\, \sigma\sqrt{t}\right) \ . \tag{57}$$

with probability density function

$$\frac{1}{x\sigma\sqrt{2\pi t}} \exp\left(-\frac{(\ln\left(\frac{x}{X_0}\right) - (\mu - \frac{1}{2}\sigma^2)t)^2}{2\sigma^2 t}\right) \ . \tag{58}$$

The evolution of the paths of Brownian motions can be classified into three regimes depending on the drift parameter μ and the volatility parameter σ:

Regime 1: if $\mu < \frac{1}{2}\sigma^2$ almost all paths are converging to 0,

Regime 2: if $\mu = \frac{1}{2}\sigma^2$, at each time point t 50% of the mass is above and 50% is below the initial value,

Regime 3: if $\mu > \frac{1}{2}\sigma^2$, almost all paths diverge to ∞.

These three cases can be identified by using the relation

$$\mathbb{P}\ (X_t < V) = \Phi\left(\frac{\ln\left(\frac{V}{X_0}\right) - (\mu - \frac{1}{2}\sigma^2)t}{\sigma\sqrt{t}}\right) \ , \tag{59}$$

where Φ denotes the cumulative distribution function of the standard normal distribution. For example in case of the first regime ($\mu - \frac{1}{2}\sigma^2 < 0$), with time t the probability of X_t being smaller than any value $V \in \mathbb{R}$ converges to 1

$$\lim_{t\to\infty} \mathbb{P}\ (X_t < V) = \lim_{t\to\infty} \Phi\left(\frac{\ln\left(\frac{V}{X_0}\right)}{\sigma\sqrt{t}} - (\mu - \frac{1}{2}\sigma^2)\sqrt{t}\right) = 1 \ . \tag{60}$$

Hence, all paths are converging to 0. The two remaining cases follow by similar arguments.

The thin blue lines in Figure 1 are paths of Brownian motions for each regime. The characteristic behaviour of each regime is clearly visible in the evolution of the paths (logarithmic scale is used for the y-axis) - convergence to 0 (Figure 1a), fluctuation around the initial value (Figure 1b) and divergence to ∞ (Figure 1c). Introducing lines representing percentiles gives a better understanding of the behaviour. The thick lines illustrate the evolution of a set of percentiles (5%, 25%, 50%, 75%, 95%), i. e. how many paths are below the line at each time and how this fraction is evolving in time. In Figure 1a for example, 75% of the paths are below the red line (75-th percentile). At time t=30 the 75-th percentile has dropped to approximately 0.0035 starting from an initial value of 10.

The α-th percentile of the geometric Brownian motion is is given by

$$p_{X_t}(\alpha) = X_0 \exp\left((\mu - \frac{1}{2})t + \sigma\sqrt{t}p_{\mathcal{N}}(\alpha)\right), \tag{61}$$

where $p_{\mathcal{N}}(\alpha)$ denotes the α-th percentile of the standard normal distribution. The behaviour of the percentiles for each regime can be specified

Regime 1: For $p \leq 50\%$, all percentiles are strictly monotonously decreasing (the exponent of $p_S(p,t)$ is negative). For $p > 50\%$, the maximum of the p-th percentile occurs at

$$t_{max} = \left(\frac{\sigma p_{\mathcal{N}}(p)}{\sigma^2 - 2\mu}\right)^2 \quad \text{and} \quad p_{S_t}(p)\Big|_{t_{max}} = X_0 \exp\left(\frac{1}{2}\frac{\sigma p_{\mathcal{N}}(p)}{\sigma - 2\mu}\right) . \tag{62}$$

After reaching the maximum the p-th percentile is decreasing strictly monotonously.

Regime 2: $p_{X_t}(50\%) = X_0$ for all times t. For $p \leq 50\%$, all percentiles are strictly monotonously decreasing (the exponent of $q_S(p,t)$ is negative). If $\mu = \frac{1}{2}v$ then the 50th percentile is constant, $p_S(50\%, t) = X_0$ for all times t. It means at each time 50% of the mass is above and 50% is below the initial value X_0. Percentiles above 50% are increasing and percentiles below 50% are decreasing in time.

Regime 3: This case is similar to the first case. However, almost all paths are converging to ∞. For $p \geq 50\%$, all percentiles are strictly monotonously increasing (the exponent of $p_S(p,t)$ is positive). For $p < 50\%$, the minimum of the p-th percentile occurs at

$$t_{max} = \left(\frac{\sigma p_{\mathcal{N}}(p)}{\sigma^2 - 2\mu}\right)^2 \quad \text{and} \quad p_{X_t}(p)\Big|_{t_{max}} = X_0 \exp\left(\frac{1}{2}\frac{\sigma p_{\mathcal{N}}(p)}{\sigma^2 - 2\mu}\right) . \tag{63}$$

It might feel counter-intuitive that the Brownian motion shown in Figure 1a is a martingale and has constant expectation value. Still, almost all paths are converging to 0. One way to resolve this alleged conflict is through understanding the consequences of the geometric Brownian motion being bounded from below and having increasing variance. The increasing variance has to be sustained by increasing paths as the process has only limited range to deviate downwards. Increasing paths, however, have to be compensated by decreasing paths as the expectation value is constant. Due to the limited range, the amount of decreasing paths has to be increasing.

A.2 Geometric Ornstein-Uhlenbeck Process

A geometric Ornstein-Uhlenbeck process satisfies the following stochastic differential equation

$$dX_t = \kappa(\Theta - \ln X_t)X_t dt + \sigma X_t dW_t , \tag{64}$$

where W_t is a Brownian motion, κ is the mean-reversion speed, Θ is the drift parameter and σ the volatility parameter The solution is given by

$$X_t = X_0^{e^{-\kappa t}} \exp\left((\theta - \frac{\sigma^2}{2\kappa})(1 - e^{-\kappa t}) + \int_0^t \sigma_i e^{-\kappa(t-s)}\, dW_s\right) . \tag{65}$$

For our purpose of creating scenarios the Ornstein-Uhlenbeck process has one advantage compared to the geometric Brownian motion. It is stationary[12], which means it has a probability distribution that does not change in time. As a consequence, the percentiles of the Ornstein-Uhlenbeck process converge.

The distribution of X_t is given by

$$X_t \sim \log \mathcal{N}\left(e^{-\kappa t}\log X_t + (\theta - \frac{\sigma^2}{2\kappa})(1 - e^{-\kappa t}),\ \frac{\sigma^2}{2\kappa}(1 - e^{-2\kappa t})\right) . \tag{66}$$

Asymptotically, the distribution of X_t converges to

$$\lim_{T\to\infty} X_t \sim \log \mathcal{N}\left(\theta - \frac{\sigma^2}{2\kappa},\ \frac{\sigma^2}{2\kappa}\right) . \tag{67}$$

[12]A process is called stationary if for all times $t_1, \ldots, t_n$ and time increments h $\mathbb{P}\left((X_{t_1}, \ldots, X_{t_n}) \in A \subset \mathbb{R}^n\right) = \mathbb{P}\left((X_{t_1+h}, \ldots, X_{t_n+h}) \in A \subset \mathbb{R}^n\right)$.

As a consequence the percentiles at time T of the geometric Ornstein-Uhlenbeck process are given by

$$p_{X_t}(\alpha) = \exp\left(e^{-\kappa t}\log X_t + (\theta - \frac{\sigma^2}{2\kappa})(1-e^{-\kappa t}) + \sqrt{\frac{\sigma^2}{2\kappa}(1-e^{-2\kappa t})}p_{\mathcal{N}}(\alpha)\right) . \tag{68}$$

In the limit $T \to \infty$ the percentiles converge to

$$p_{X_t}(\alpha) = X_0 \exp\left(\theta - \frac{\sigma^2}{2\kappa} + \sqrt{\frac{\sigma^2}{2\kappa}}p_{\mathcal{N}}(\alpha)\right) . \tag{69}$$

B CP-DOTO Equilibria and Properties

From the perspective of arbitrage traders two cases are profitable:

1. $(1-\rho)X_g^c(t) > P_t$ which is equivalent to $X_c^u(t) = X_g^u(t)X_g^c(t) < 1-\rho$
2. $X_g^c(t) < (1-\rho)P_t$ which is equivalent to $X_c^u(t) = X_g^u(t)X_g^c(t) > \frac{1}{1-\rho}$.

In both cases we are assuming that arbitrage traders will take advantage of the arbitrage opportunity until it vanishes at time t_e, i.e. until either $(1-\rho)X_g^c(t_e) = P_{t_e}$ or $X_g^c(t_e) = (1-\rho)P_{t_e}$. We refer to each of these states as the equilibrium state.

In the first case the equilibrium state is described by the following set of equations of unknown time t_e quantities:

$$(1-\rho)X_g^c(t_e) = P_{t_e} \tag{70}$$
$$C^r(t_e)G^r(t_e) = C^r(t)G^r(t) \tag{71}$$
$$C^r(t_e) - C^r(t) = (1-\rho)(C^m(t) - C^m(t_e)) \tag{72}$$
$$G^r(t_e) + G^m(t_e) = G^r(t) + G^m(t) . \tag{73}$$

The set of equations can be solved to give solutions with regard to time t quantities

$$P_{t_e} = \frac{C^r(t) + (1-\rho)C^m(t)}{G^r(t) + G^m(t)} \tag{74}$$
$$G^r(t_e) = G^r(t)\sqrt{\frac{P_t}{P_{t_e}}} \tag{75}$$
$$C^r(t_e) = C^r(t)\sqrt{\frac{P_{t_e}}{P_t}} \tag{76}$$
$$G^m(t_e) = \left(1 - \sqrt{\frac{P_t}{P_{t_e}}}\right)G^r(t) + G^m(t) \tag{77}$$
$$C^m(t_e) = \frac{1-\sqrt{\frac{P_{t_e}}{P_t}}}{1-\rho}C^r(t) - C^m(t) . \tag{78}$$

In the second case the equilibrium state is described by a similar set of unknown time t_e quantities:

$$X_g^c(t_e) = (1-\rho)P_{t_e} \tag{79}$$
$$C^r(t_e)G^r(t_e) = C^r(t)G^r(t) \tag{80}$$
$$C^r(t_e) + C^m(t_e) = C^r(t) + C^m(t) \tag{81}$$
$$G^r(t_e) - G^r(t) = (1-\rho)(G^m(t) - G^m(t_e)) . \tag{82}$$

The set of equations can be solved to give solutions with regard to time t quantities

$$P_{t_e} = \frac{C^r(t) + C^m(t)}{G^r(t) + (1-\rho)G^m(t)} \tag{83}$$

$$G^r(t_e) = G^r(t)\sqrt{\frac{P_t}{P_{t_e}}} \tag{84}$$

$$C^r(t_e) = C^r(t)\sqrt{\frac{P_{t_e}}{P_t}} \tag{85}$$

$$G^m(t_e) = \frac{1-\sqrt{\frac{P_t}{P_{t_e}}}}{1-\rho}G^r(t) + G^m(t) \tag{86}$$

$$C^m(t_e) = \left(1-\sqrt{\frac{P_{t_e}}{P_t}}\right)C^r(t) + C^m(t)\ . \tag{87}$$

In both cases the Celo Dollar price $X_g^u(t_e)$ at t_e follows from $X_g^u(t) = \frac{U}{C^m(t_e)}$.

Observation 1.

i) If $(1-\rho)X_g^c(t) > P_t$, then $P_t < P_{t_e} < (1-\rho)X_g^c(t)$.

ii) If $X_g^c(t) < (1-\rho)P_t$, then $\frac{1}{1-\rho}X_g^c(t) < P_{t_e} < P_t$.

Proof. We prove the second statement. Assume $X_g^c(t) < (1-\rho)P_t$.

$$X_g^c(t) < (1-\rho)P_t \quad \Rightarrow \quad \frac{C^m(t)}{G^m(t)} < (1-\rho)\frac{C^r(t)}{G^r(t)} \quad \Rightarrow \quad \frac{C^m(t)}{C^r(t)} < (1-\rho)\frac{G^m(t)}{G^r(t)} \tag{88}$$

First, we are show $\frac{P_{t_e}}{P_t} < 1$:

$$\frac{P_{t_e}}{P_t} = \frac{G^r(t)}{C^r(t)}\frac{C^r(t)+C^m(t)}{G^r(t)+(1-\rho)G^m(t)} = \frac{1+\frac{C^m(t)}{C^r(t)}}{1+(1-\rho)\frac{G^m(t)}{G^r(t)}} \overset{(88)}{<} \frac{1+\frac{C^m(t)}{C^r(t)}}{1+\frac{C^m(t)}{C^r(t)}} = 1 \tag{89}$$

Next we show $\frac{P_{t_e}}{X_g^c(t)} > \frac{1}{1-\rho}$:

$$\frac{P_{t_e}}{X_g^c(t)} = \frac{G^m(t)}{C^m(t)}\frac{C^r(t)+C^m(t)}{G^r(t)+(1-\rho)G^m(t)} = \frac{1+\frac{C^r(t)}{C^m(t)}}{1-\rho+\frac{G^r(t)}{G^m(t)}} \overset{(88)}{>} \frac{1+\frac{C^r(t)}{C^m(t)}}{1-\rho+(1-\rho)\frac{C^r(t)}{C^m(t)}} = \frac{1}{1-\rho} \tag{90}$$

This proves the second statement. The first statement can be proven by similar arguments. □

Observation 2.

i) If $(1-\rho)X_g^c(t) > P_t$, then P_{t_e} is strictly decreasing with regard to $G^r(t)$.

ii) If $X_g^c(t) < (1-\rho)P_t$, then P_{t_e} is strictly increasing with regard to $G^r(t)$.

Proof. We prove the second statement. Assume $X_g^c(t) < (1-\rho)P_t$.

$$X_g^c(t) = \frac{C^m(t)}{G^m(t)} < (1-\rho)P_t \quad \Rightarrow \quad (1-\rho)P_tG^m(t) - C^m(t) > 0 \tag{91}$$

The derivative of $P_{t_e} = \frac{C^r(t)+C^m(t)}{G^r(t)+(1-\rho)G^m(t)}$ is given by

$$\frac{d}{dG^r(t)}P_{t_e} = \frac{d}{dG^r(t)}\left(\frac{C^r(t)+C^m(t)}{G^r(t)+(1-\rho)G^m(t)}\right) \tag{92}$$

$$= \frac{d}{dG^r(t)}\left(\frac{P_tG^r(t)+C^m(t)}{G^r(t)+(1-\rho)G^m(t)}\right) = \frac{(1-\rho)P_tG^m(t)-C^m(t)}{\left(G^r(t)+(1-\rho)G^m(t)\right)^2} \overset{(91)}{>} 0 \tag{93}$$

It follows that P_{t_e} is strictly increasing with regard to $G^r(t)$. The first statement can be proven by similar arguments. □

Observation 3.
With regard to $G^r(t)$ the limit of the equilibrium price P_{t_e} is given by

$$\lim_{G^r(t)\to\infty} P_{t_e} = P_t \ . \tag{94}$$

Proof. Assume $X_g^c(t) < (1-\rho)P_t$. Then

$$\frac{P_{t_e}}{P_t} = \frac{1+\frac{C^m(t)}{C^r(t)}}{1+(1-\rho)\frac{G^m(t)}{G^r(t)}} = \frac{1+\frac{C^m(t)}{P_tG^r(t)}}{1+(1-\rho)\frac{G^m(t)}{G^r(t)}} = \frac{1}{1+(1-\rho)\frac{G^m(t)}{G^r(t)}} + \frac{1\frac{C^m(t)}{P_tG^r(t)}}{1+(1-\rho)\frac{G^m(t)}{G^r(t)}} \tag{95}$$

$$= \frac{1}{1+(1-\rho)\frac{G^m(t)}{G^r(t)}} + \frac{\frac{C^m(t)}{P_t}}{G^r(t)+(1-\rho)G^m(t)} \overset{G^r(t)\to\infty}{\to} 1+0 \ . \tag{96}$$

Assume $(1-\rho)X_g^c(t) < P_t$. Then

$$\frac{P_{t_e}}{P_t} = \frac{1+(1-\rho)\frac{C^m(t)}{C^r(t)}}{1+\frac{G^m(t)}{G^r(t)}} = \frac{1+(1-\rho)\frac{C^m(t)}{P_tG^r(t)}}{1+\frac{G^m(t)}{G^r(t)}} = \frac{1}{1+\frac{G^m(t)}{G^r(t)}} + \frac{(1-\rho)\frac{C^m(t)}{P_tG^r(t)}}{1+\frac{G^m(t)}{G^r(t)}} \tag{97}$$

$$= \frac{1}{1+\frac{G^m(t)}{G^r(t)}} + \frac{(1-\rho)\frac{C^m(t)}{P_t}}{G^r(t)+G^m(t)} \overset{G^r(t)\to\infty}{\to} 1+0 \ . \tag{98}$$

□

Observation 4.

i) If $(1-\rho)X_g^c(t) > P_t$, then

$$\lim_{G^r(t)\to\infty} X_c^u(t_e) = \frac{2X_c^u(t)}{1+\frac{1}{1-\rho}\frac{P_t}{X_g^c(t)}} \ .$$

If $X_c^u(t) = \frac{P_t}{X_g^c(t)}$ after an oracle update, then

$$\lim_{G^r(t)\to\infty} X_c^u(t_e) = \frac{2}{\frac{1}{1-\rho}+X_u^c(t)} \ .$$

ii) If $X_g^c(t) < (1-\rho)P_t$, then

$$\lim_{G^r(t)\to\infty} X_c^u(t_e) = \frac{2X_c^u(0)}{1+(1-\rho)\frac{P_t}{X_g^c(t)}} \ .$$

If $X_c^u(t) = \frac{P_t}{X_g^c(t)}$ after an oracle update, then

$$\lim_{G^r(t)\to\infty} X_c^u(t_e) = \frac{2}{(1-\rho)+X_u^c(t)} \ .$$

Proof. We prove the first statement. We calculate $\lim_{G^r(t)\to\infty} C^m(t_e)$ and use $C^m(t_e) = C^m(t) - \frac{1}{1-\rho}\left(C^r(t_e) - C^r(t)\right)$.

$$C^r(t_e) - C^r(t) = C^r(t)\sqrt{\frac{P_{t_e}}{P_t}} - C^r(t) \tag{99}$$

$$= P_tG^r(t)\sqrt{\frac{G^r(t)+(1-\rho)\frac{C^m(t)}{P_t})}{G^r(t)+G^m(t)}} - P_tG^r(t) \tag{100}$$

$$= P_tG^r(t)\sqrt{1-\frac{G^r(t)+G^m(t)}{G^r(t)+G^m(t)}+\frac{G^r(t)+(1-\rho)\frac{C^m(t)}{P_t})}{G^r(t)+G^m(t)}} - P_tG^r(t) \tag{101}$$

$$= P_tG^r(t)\sqrt{1+\frac{\frac{1-\rho}{P_t}C^m(t)-G^m(t)}{G^r(t)+G^m(t)}} - P_tG^r(t) \tag{102}$$

$$= P_tG^r(t)\left(1+\frac{1}{2}\frac{\frac{1-\rho}{P_t}C^m(t)-G^m(t)}{G^r(t)+G^m(t)}+\mathcal{O}(\frac{1}{G^r(t)})-1\right) \tag{103}$$

In the limit, the difference of the Celo Dollar wallet at time t and t_e converges to

$$\lim_{G^r(t)\to\infty}(C^r(t_e)-C^r(t))=\frac{1}{2}\left((1-\rho)C^m(t)-P_tG^m(t)\right)\ . \tag{104}$$

Therefore, the Celo Dollar market tank is given by

$$\lim_{G^r(t)\to\infty}C^m(t_e)=C^m(t)-\frac{1}{1-\rho}\frac{1}{2}\left((1-\rho)C^m(t)-P_tG^m(t)\right)=\frac{1}{2}\left(C^m(t)+\frac{P_tG^m(t)}{(1-\rho)}\right) \tag{105}$$

The Celo Dollar price is given by

$$X_c^u(t_e)=\frac{U}{C^m(t_e)}\overset{G^r(t)\to\infty}{\to}\frac{U}{\frac{1}{2}\left(C^m(t)+\frac{P_tG^m(t)}{(1-\rho)}\right)}=\frac{2\frac{U}{C^m(t)}}{1+\frac{P_t}{1-\rho}\frac{G^m(t)}{C^m(t)}}=\frac{2X_g^u(t)}{1+\frac{1}{1-\rho}\frac{P_t}{X_g^c(t)}}\ .$$

The second statement can be proven by similar arguments. □

B.1 Parameters for Figures 8 - 10b

Parameter	**Fig. 8**	**Fig. 9**	**Fig. 10a**	**Fig. 10b**
Tank U	10 000	10 000 / 100 000	100 000 000	100 000 000
X_g^u	2	2	2	2
X_g^c	3	3	3	3
Fee ρ	0.05	0.05	0.05	0.05
Fraction ϕ^r	0.001	0.001	0.1	0.001
Reserve CELO	100 000 000	100 000 000	100 000 000	100 000 000
P	2	2	$\frac{1}{5}X_g^u(t)^*$	$\frac{1}{5}X_g^u(t)^*$
Iterations	15	20	100	100

Table 3: The table contains the parameters that have been used to generate the examples in Figures 8 - 10b. On-chain CELO prices P with a * are assumed to be affected by oracle manipulation: Instead of the true CELO market price $X_g^u(t)$ the value $\frac{1}{5}X_g^u(t)$ is used to update the on-chain price $P_t := \frac{1}{5}X_g^u(t)$.

C CP-DOTO Parameter Setting

	Parameter	Settings	Explanation
Demand	Q_0	20 000 000	Initial value
	κ_d	0.001	Mean reversion speed
	σ_d	100%	Volatility
	Θ_d	$Q_0 + \frac{\sigma_d^2}{2\kappa_d}$	Drift
	μ^d_{idio}	0%	Mean parameter for idiosyncratic jump size
	σ^d_{idio}	30%	Volatility of idiosyncratic jump size
	λ^d_{idio}	5	Idiosyncratic jump intensity
	$\mu_{\rho_{d,a}}$	0.5	Mean of correlation btw. demand and crypto assets
	$\sigma_{\rho_{d,a}}$	0.05	Volatility of correlation btw. demand and crypto assets
Cryptomarket	A_0	1	Initial value
	κ_a	0.001	Mean reversion speed
	σ_a	100%	Volatility of demand
	Θ_a	$Q_0 + \frac{\sigma_d^2}{2\kappa_d}$	Drift
	μ^a_{idio}	0%	Mean parameter idiosyncratic jump size
	σ^a_{idio}	30%	Volatility of idiosyncratic jump size
	λ^a_{idio}	5	Idiosyncratic jump intensity
	μ^a_{syst}	0%	Mean parameter systematic jump size
	σ^a_{syst}	30%	Volatility of systematic jump size
	λ^a_{syst}	2	Systematic jump intensity
Protocol & Macro	v	20	Annual velocity of Celo Dollars
	s	0.5%	Stability fee
	r	25%	Discount rate
	f	0.2%	Utility fee
	$\hat{\mu}$	27.46%	Market expected Celo Dollar Growth
	N	3	Number of non-Celo reserve assets
	r^g	0.5	Target percentage of CELO in the reserve
	ν	10%	Ownership dilution per annum
	ρ	0.5%	Spread for CP-DOTO transactions
	f_{bal}	14	Rebalancing frequency
	ϕ^r	0.1	Reserve fraction
	f_{update}	$\frac{1}{24}$	Daily update frequency of CP-DOTO
	G^{total}	1 000 000 000	Total number of CELO coins
	$G^{reserve}$	120 000 000	Initial number of CELO coins in the reserve
	λ_{def}	3%	Initial default probability of non-volatile assets
	τ^d	0.5	Reserve threshold Celo Dollar demand spiral
	τ^g	0.5	Reserve threshold CELO price spiral
	τ^r_1	0.75	Reserve threshold 100% non-volatile assets
	τ^r_0	1.5	Reserve threshold 0% non-volatile assets

Table 4: This table gives an overview over the main parameters used in this simulation analysis. Many of these parameter choices are subjective and different choices will necessarily lead to different stability results. Protocol related parameter choices might not coincide with the protocol parameters at launch of the network.